Annual Letter Report

Growth, Characterization and Device Development in Monocrystalline Diamond Films

Supported by the Innovative Science and Technology Office
Strategic Defense Initiative Organization
Office of Naval Research
under Contract #N00014-90-J-1604
for the period January 1, 1991–December 31, 1991

Robert F. Davis, Klaus J. Bachmann, Jeffrey T. Glass,
R. J. Nemanich* and R. J. Trew**
L. Bergman*, T. P. Humphreys*, G.-H. M. Ma, B. R. Stoner,
K. F. Turner*, J. VanderWeide*, S. D. Wolter
North Carolina State University
c/o Materials Science and Engineering Department
*Department of Physics
**Electrical and Computer Engineering
Raleigh, NC 27695

December 31, 1991

REPORT DOCUMENTATION PAGE

Form Approved
OMB No 0704-0188

1. AGENCY USE ONLY (Leave blank)	2. REPORT DATE	3. REPORT TYPE AND DATES COVERED
	December, 1991	Annual Letter 1/1/91–12/31/91

4. TITLE AND SUBTITLE
Growth, Characterization and Device Development in Monocrystalline Diamond Films

5. FUNDING NUMBERS
s400003srr08
1114SS
N00179
N66005
4B855

6. AUTHOR(S)
Robert F. Davis

7. PERFORMING ORGANIZATION NAME(S) AND ADDRESS(ES)
North Carolina State University
Hillsborough Street
Raleigh, NC 27695

8. PERFORMING ORGANIZATION REPORT NUMBER
N00014-90-J-1604

9. SPONSORING/MONITORING AGENCY NAME(S) AND ADDRESS(ES)
Department of the Navy
Office of the Chief of Naval Research
800 North Quincy Street, Code 1513:CMB
Arlington, VA 22217-5000

10. SPONSORING/MONITORING AGENCY REPORT NUMBER

11. SUPPLEMENTARY NOTES

12a. DISTRIBUTION/AVAILABILITY STATEMENT
Approved for Public Release; Distribution Unlimited

12b. DISTRIBUTION CODE

13. ABSTRACT (Maximum 200 words)

The nucleation of diamond grains on unscratched Si(100) wafer is enhanced by four order of magnitude relative to scratched substrates by using negative bias-enhanced microwave plasma CVD in a 2% methane/hydrogen plasma for an initial period. In vacuo surface analysis has revealed that the actual nucleation occurs on the amorphous C coating present on the thin SiC layer which forms as the product of the initial reaction with the Si surface. It is believed that the C forms critical clusters which are favorable for diamond nucleation. Similar enhancement was observed together with the occurrence of textured diamond films in the use of bias pretreatment of cubic β-SiC substrates. Approximately 50% of the initial diamond nuclei were aligned with the SiC substrate. In contrast, the use of the biasing pretreatment for one hour on polycrystalline substrates resulted in only about 7% coverage with diamond particles. Numerous techniques have been used to analyze the nucleation and growth phenomena, especially micro-Raman and scanning tunneling microscopy. The latter technique has shown that the morphology of doped and undoped diamond nuclei are similar, as well as the fact that significant concentrations of vacancy related defects are present. In device-related studies, uv-photoemission studies have shown that TiC occurs at the Ti-diamond (100) interface after a 400°C anneal. The Schottky barrier height from this metal on p-type diamond was determined to be 1.0 ± 0.2 eV. Indications of negative electron affinity (NEA) was observed and attributed to emission of electrons that are quasi-thermalized to the bottom of the conduction band. A disordered surface removes the NEA. The microwave performance of p-type (β-doped) diamond MESFETs at 10 GHz has been further investigated. Elevated temperatures may be necessary to obtain sufficient free charge densities in the conducting channel but this will result in degraded device performance. Each of these sections are self-contained including the pertinent references.

14. SUBJECT TERMS
diamond thin films, plasma enhanced chemical vapor deposition, Raman spectroscopy, scanning tunneling microscopy, Ti Schottky contacts, uv photoemission, epitaxial growth, amorphous C films, electronic devices, MESFETS

15. NUMBER OF PAGES
98

16. PRICE CODE

17. SECURITY CLASSIFICATION OF REPORT	18. SECURITY CLASSIFICATION OF THIS PAGE	19. SECURITY CLASSIFICATION OF ABSTRACT	20. LIMITATION OF ABSTRACT
UNCLAS	UNCLAS	UNCLAS	SAR

NSN 7540-01-280-5500

Standard Form 298 (Rev. 2-89)
Prescribed by ANSI Std. Z39-18
298-102

Table of Contents

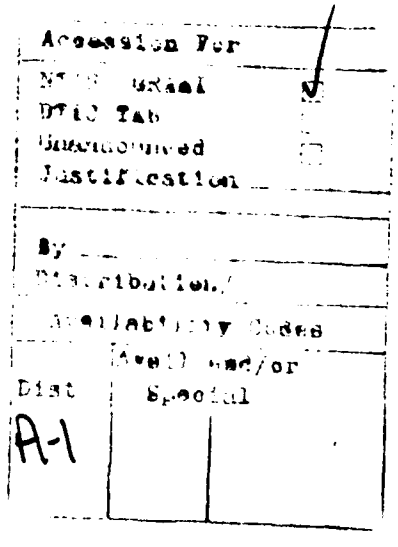

I. Introduction

Diamond has an unusual combination of extreme properties which make it a strategic material. It is an excellent material for abrasive and wear resistant surfaces, tool coatings, and corrosion barriers because of its high hardness, strength, chemical resistance, and low coefficient of friction. The UV-visible-IR transparency makes diamond an interesting material for optical applications, such as windows, lens coatings, and X-ray lithography masks. Furthermore, its high thermal conductivity makes diamond films an ideal heat diffuser material for high temperature, high power semiconductor devices, thus allowing a high degree of circuit integration and denser packaging of the devices without thermal problems. The high hole mobility, the wide band gap and the high breakdown voltage of doped diamond may ultimately lead to active semiconductor diamond elements for high power/high frequency electronic devices and devices to be utilized in high temperature, chemically harsh and/or high radiation flux environments that complement the current silicon (Si) and gallium arsenide (GaAs) technologies. Indeed, the Johnson [1] and Keyes [2] figures of merit for high frequency/high power and high frequency/high packing density applications, respectively, indicate that diamond has 1189 and 70 times the potential of GaAs [3]. More recently, computer modeling of MESFET structures using a large signal device simulator [4] has qualitatively supported the potential superiority of diamond over GaAs or any other current or proposed semiconductors with respect to RF power output. However, to realize the true potential of diamond in all of the aforementioned applications, from tool coatings to high power devices, films and/or coatings of diamond must be obtained on nondiamond substrates in an economically viable manner. Such diamond films and coatings have recently been achieved throughout the world using low-pressure chemical vapor deposition (CVD) in contrast to the high pressure, high temperature synthesis previously used to form bulk diamond. However, to date, single crystal diamond films have not been grown on non-diamond substrates—an important and necessary step, if reproducible and commercially viable diamond semiconductor devices are to be produced.

In this reporting period, the research efforts have concentrated in several areas: bias-enhanced nucleation and growth of diamond on Si(001), polycrystalline Cu and β-SiC(001); Raman and optical, scanning electron and scanning tunneling microscopies of the nuclei and films; interface reaction between Ti and diamond; and the modeling and characterization of MESFET devices fabricated in diamond. The following subsections give the experimental details of this research, provide discussions and conclusions regarding these studies and describe the plans for future research.

References

1. E. O. Johnson, *RCA Review*, **26** 163, (1965).
2. R. W. Keyes, *Proc. IEEE*, **60** 225, 1972.
3. R. Roy, *Nature*, **325** 17, 1987.
4. R. J. Trew and J. B. Yuan, "The prospect of a powerful diamond MESFET," presented at the Third Annual Diamond Technology Initiative Symp., Crystal City, VA July 12-14, 1988.

II. Characterization of Bias-Enhanced Nucleation of Diamond on Silicon by In Vacuo Surface Analysis and Transmission Electron Microscopy*

B. R. Stoner, G.-H. M. Ma, S. D. Wolter, and J.T. Glass
Department of Materials Science and Engineering
North Carolina State University, Raleigh, NC 27695-7907

Abstract

An indepth study has been performed of the nucleation of diamond on silicon by bias-enhanced microwave plasma chemical vapor deposition. Substrates were pretreated by negative biasing in a 2% methane/hydrogen plasma. The bias pretreatment enhanced the nucleation density on unscratched silicon wafers up to 10^{11} /cm^2 as compared with 10^7/cm^2 on scratched wafers. In-vacuo surface analysis including XPS, AES and XPS-EELS were used to systematically study both the initial nucleation and growth processes. High resolution cross sectional TEM was used to study the physical and structural characteristics of the diamond/silicon interface as well as compliment and enhance the in-vacuo surface analytical results. Raman spectroscopy confirmed that diamond was actually nucleating during the bias-pretreatment. SEM has shown that once the bias is turned off, and conventional growth is conducted, diamond grows on the existing nuclei and no continued nucleation occurs. If the bias is left on throughout the entire deposition, the resulting film will be of much poorer quality than if the bias had been turned off and conventional growth allowed to begin.

Intermittent surface analysis showed that a complete silicon carbide layer developed before diamond could be detected. High resolution XTEM confirmed that the interfacial layer was amorphous and varied in thickness from 10 to 100 Å. A small amount of amorphous carbon is detected on the surface of the silicon carbide and it is believed to play a major role in the nucleation sequence. A model is proposed to help explain bias-enhanced nucleation on silicon, in hopes that this will improve the understanding of diamond nucleation in general and eventually result in the nucleation and growth of better quality diamond films.

Due to budget constraints in the printing of the 1991 Annual Letter Report, we are unable to send this entire article (pages 3 through 39) in the report that is mailed to all on the Distribution List (see Appendix B). However, we would be happy to honor personal requests. If you would like a copy of the complete article, please send a request to the authors at the above address.

* Preprint of paper submitted to Phys. Rev. B

III. Substrate Effects on Bias-enhanced Diamond Nucleation; Polycrystalline Cu vs. Si(100)

A. Introduction

It has been observed that the properties inherent to the substrate have an influence on the diamond nucleation phenomenon. Past research has indicated that the time prior to the formation of the initial nuclei (ie. the incubation time) and the rate at which the nuclei are formed vary depending on the substrate material used.[1,2] Though much work has been involved in the study of the growth mechanisms, a thorough understanding of the nucleation phenomenon is lacking and is essential to the fabrication of high quality diamond films. Once models for the nucleation of diamond are established, it may then be possible to provide conditions ideal for heteroepitaxial nucleation and growth.

When considering suitable foreign substrates for diamond growth, two classes of substrate materials arise; carbide and non-carbide formers. These two classes are derived based on the fact that they seem to formulate two separate types of nucleation phenomena. Though diamond can be grown on either type of material, there appear to be similarities and dissimilarities in the individual nucleation mechanisms. The basic similarities are; (i) some type of interfacial carbon-based structure is present prior to nucleation and (ii) there exists an induction time before initial nucleation. The basic dissimilarities are; (i) the carbide forming substrates have some type of amorphous carbon saturated on a carbidtic surface prior to nucleation while the non-carbide forming substrates have a highly graphitic component present and (ii) the incubation time is influenced by the rate at which the carbide is formed for the carbide forming substrates as compared to the non-carbide forming substrates where the incubation time is possibly shorter due to the formation of its graphitic interfacial layer.

This study was performed to fully characterize diamond nucleation on both carbide and non-carbide forming substrates. Stoner et al[3] reported enhanced nucleation of diamond on Si(100) utilizing a biasing pretreatment step and subsequently investigated the nucleation phenomenon responsible for the enhanced nucleation. The same experimental conditions maintained in the work performed on the Si(100) will be used to study the nucleation phenomenon of diamond grown on polycrystalline copper. A comparison of these two studies should yield a better understanding of diamond nucleation in general.

B. Experimental Procedure

1. The Growth and Analytical System

Low pressure diamond growth was performed using microwave plasma chemical vapor deposition (MPCVD) on large-grained polycrystalline copper substrates. The growth system is adjoined to an analytical system by way of a transfer tube, thus making it possible to perform

in situ surface analysis. A complete description of the growth and analytical system has been previously documented.[3]

2. Sample Preparation

The polycrystalline copper substrates were 1cm × 1cm in dimension with a grain size of typically 40μm in diameter. The samples were polished using 600 grit SiC followed by 30μm, 6μm, and then 1μm diamond paste. The samples were further polished to remove any other defects and residual diamond with .3μm followed by .05μm Al_2O_3. The substrates were subsequently cleaned in TCE, acetone, methanol, propanol and, finally, rinsed thoroughly in deionized(DI) water. Prior to placing the samples into the chamber an HCl:DI etch was performed to ensure that the least amount of oxygen would be present on the substrate.

3. Test of Biasing Effects on Nucleation

Biasing times of 1, 2, and 3 hours were chosen to observe the nucleation density as a function of predeposition biasing time. Scanning electron microscopy (SEM) was used for this purpose. During this procedure the substrates were immersed in a CH_4/H_2 plasma with a chamber pressure of typically 15 torr and a CH_4/H_2 ratio of 2%. The substrates were negatively biased by maintaining a current, induced by the positively ionized species, of typically 100mA. Table 1 lists the conditions under which the biasing pretreatment step was performed.

Table 1.	Biasing Conditions	Growth Conditions
Microwave Power	~600 watts	~600 watts
CH_4/H_2	2.0%	1.0%
Pressure (Torr)	15	25
Substrate Temperature (°C)	~650	~600
Bias Voltage	-250VDC	Floating
Bias Current	~100mA	N/A
Sample Position	Immersed	Immersed

4. Surface Analytical Series vs. Bias Time

This series of runs investigated the form and amount of carbon (and oxygen) present on the copper surface at 0.25 hour intervals within a 1 hour bias period. After each of these 0.25 hour bias times, x-ray photoelectron spectroscopy (XPS), Auger electron spectroscopy (AES), and electron energy loss spectroscopy (EELS) were performed to characterize the carbon present on the copper surface early in the nucleation process.

C. Results and Discussion

1. Biasing Results of Deposition on Polycrystalline Copper as compared to Si(100)

The nucleation density after a 1 hour predeposition biasing time followed by an extended amount of growth is much greater on the Si(100) than on the polycrystalline copper. In Figure 1(a), a complete surface coverage of diamond on the Si(100) surface is evident while in Figure 1(b) the polycrystalline copper surface coverage is considerably less (ie. roughly 7%). The nucleation density versus predeposition biasing time indicated a high nucleation rate for diamond grown on Si(100).[3] In fact, it was possible to obtain complete surface coverage after roughly 2 hours of biasing. The polycrystalline copper, however, yields a considerably lower nucleation rate. A plot of the nucleation density versus predeposition biasing time for both substrates is displayed in Figure 2.

2. Surface Analytical Series vs. Bias Time

An XPS bias time series was performed to investigate what elements were present on the polycrystalline copper substrate after each of the 0.25 hour bias intervals. A survey scan only indicated carbon present on the surface; therefore, it was possible to determine the carbon layer thickness by performing deconvolution of the Cu(2p3/2). A layer thickness of 5 to 15Å was calculated throughout each of the bias intervals, and it appears that the carbon layer thickness stops increasing as early as 0.25 hours. This approximation of thickness is based on an assumed layer-by-layer growth with an inelastic electron mean free path of 15Å. The AES bias time series indicated that some type of graphite dominates the surface at each bias interval as shown in Figure 3. The "graphite" appears to become less ordered at longer bias times due to the distinctive graphite shoulder at roughly 260eV diminishing. Graphite on the other hand, was not detected on the Si(100) surface up to the resolution of the system. The type of carbon structure determined by the use of EELS agrees well with the AES data in the respect that some type of graphitic carbon exists (Figure 4). Again, as early a 0.25 hours, the structure of the carbon looks generally the same throughout each biasing step.

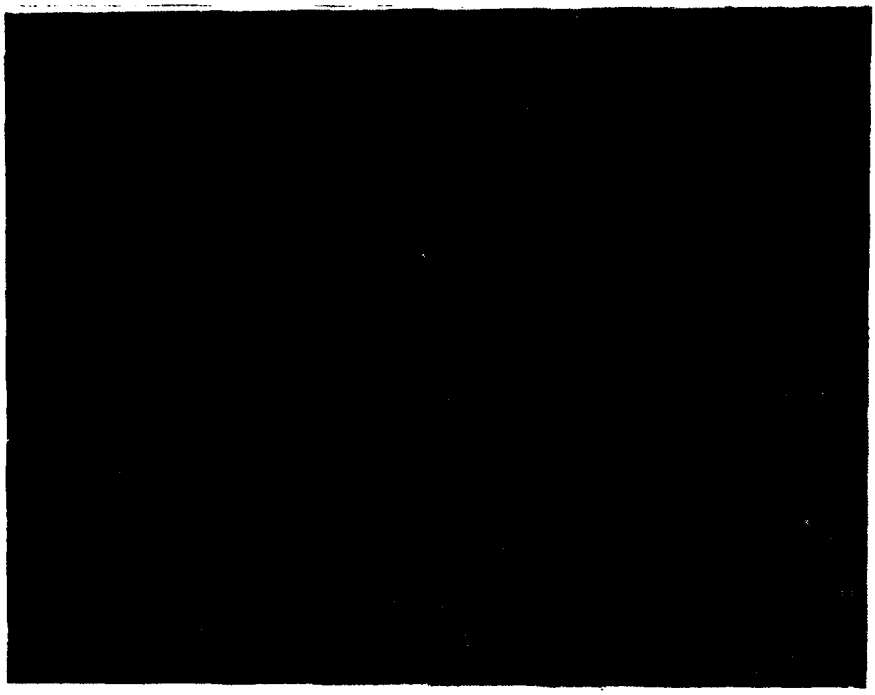

Figure 1(a). Surface coverage of diamond on Si(100) surface.

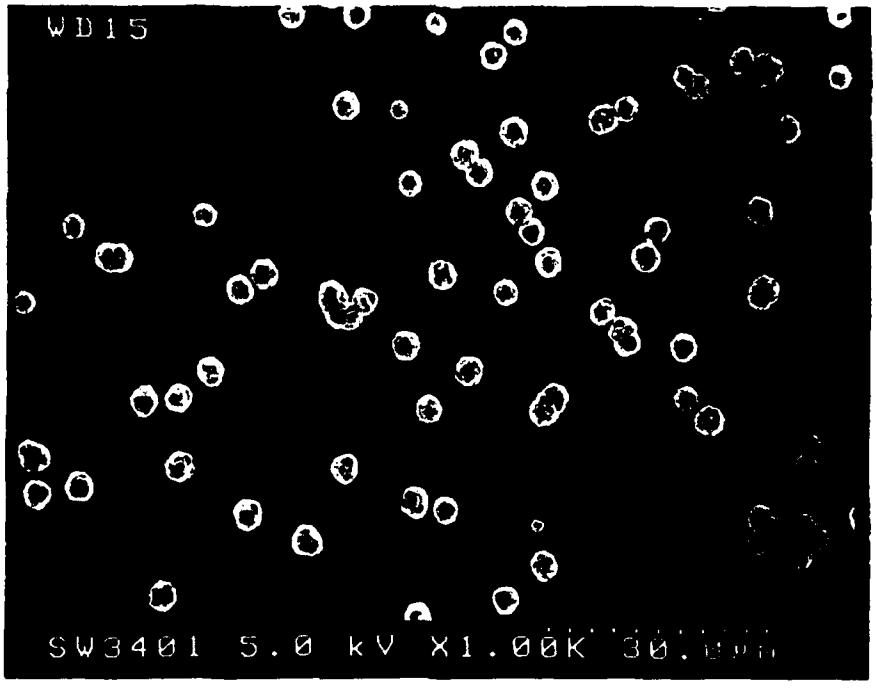

Figure 1(b). Polycrystalline copper surface coverage.

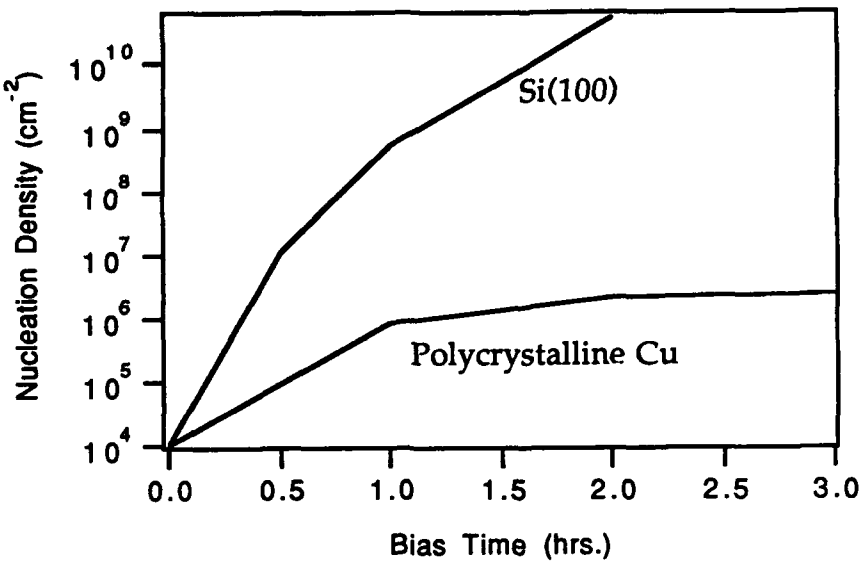

Figure 2. Plot of nucleation density versus predeposition biasing time.

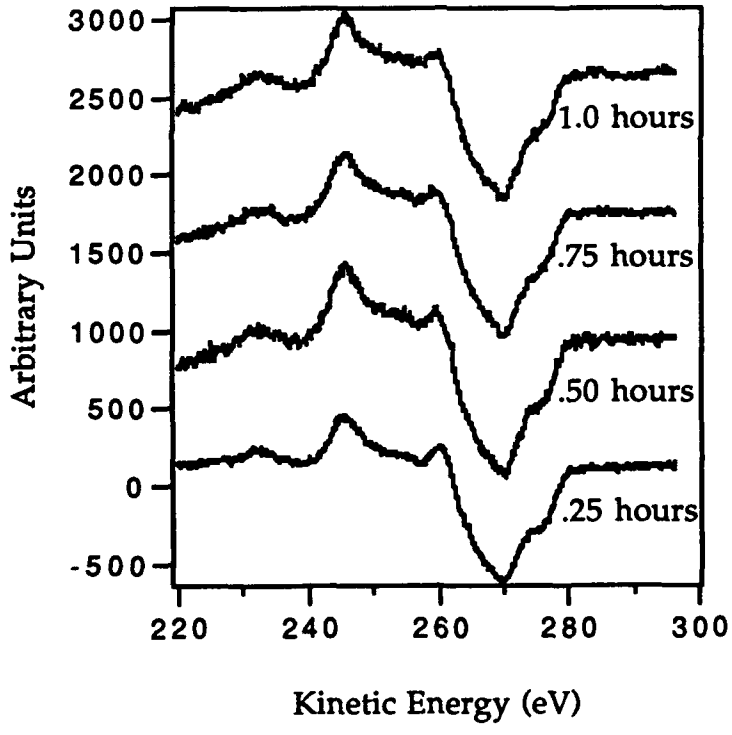

Figure 3. AES bias time series indicates that some type of graphite dominates the surface at each bias interval.

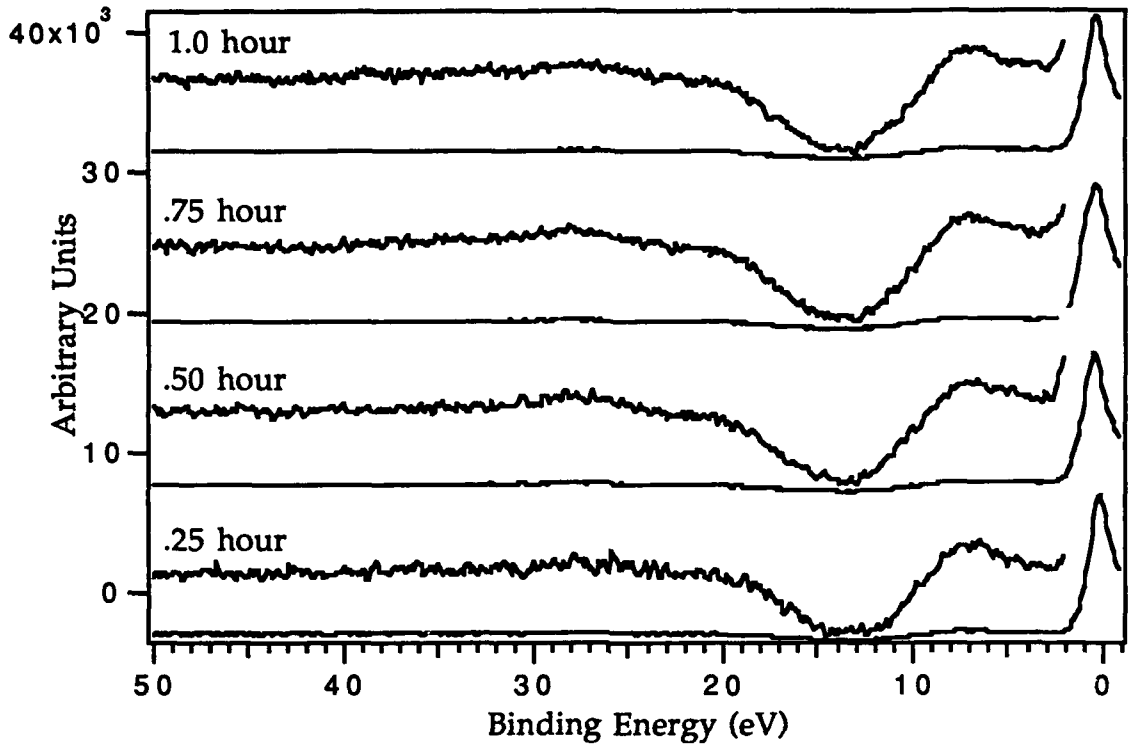

Figure 4. Presence of graphitic carbon.

D. Conclusions

The carbon-based interfacial layer on the polycrystalline copper is generally 5 to 15Å thick throughout each bias interval. This implies that the interfacial layer thickness does not increase, but rather stops growing very early. This layer has a graphitic structure as was investigated by the use of AES and EELS. The Si(100) interfacial layer was characterized by formation of a carbide with some type of non-diamond carbon present at the surface. The type of interfacial layer that develops on these two substrates prior to diamond nucleation has an influence on the diamond nucleation density as well as the rate of nucleation.

E. Future research plans/goals

It is the intention of this author to obtain an increased knowledge base with respect to the diamond nucleation phenomenon. This will be attempted by investigating diamond nucleation on a variety of substrate materials such as Mo, Ti, Ni, Ta, Ge, etc... . These substrate materials may be classified as carbide and non-carbide formers. Several overall trends will be studied among the substrate materials such as (1) the type of interlayer that develops, (2) the incubation time, (3) the nucleation density, and (4) the diamond morphology. The trends established among the carbide and non-carbide formers may lead to a better understanding of the surface conditions that must exist as well as the inherent properties that the substrate

material must exhibit to obtain a high nucleation density and high nucleation rate. With a better understanding of the diamond nucleation phenomenon it will be possible to apply this knowledge to the heteroepitaxial growth of diamond.

F. References

1. P. O. Joffreau, R. Haubner, B. Lux, Presented at MRS Spring Meeting, Reno, Nevada, April 5-9, 1988.
2. B. V. Spitsyn, L. L. Bouilov, B. V. Deryaguin, J. Cryst. Growth **52**, 219-226 (1981).
3. B. R. Stoner, G.-H. M. Ma, S. D. Wolter, J. T. Glass, submitted to Phys. Rev. B, (1991).

IV. Textured Diamond Growth on (100) β-SiC via Microwave Plasma CVD*

B. R. Stoner and J.T. Glass
Department of Materials Science and Engineering,
North Carolina State University, Raleigh, NC 27695-7907

Textured diamond films have been deposited on b-SiC via microwave plasma CVD preceded by a an in-situ bias pretreatment that enhances nucleation. Approximately 50% of the initial diamond nuclei appear to be aligned with the C(001) planes parallel to the SiC(001), and C<110> directions parallel to the SiC<110> within 3°. The diamond was characterized by Raman spectroscopy, RHEED, and SEM.

I. Introduction

The promise that diamond thin films show for electronic applications has been made clear.[1, 2] However its promising electronic properties are based on the bulk properties of diamond, and for it to be fully utilized as a semiconductor material from which to fabricate electronic devices, it is necessary to produce single crystal thin films over large areas[3-6]. Homoepitaxial growth of diamond has been reported, however, substrates of sufficient size to make the process economical are not available. The growth of heteroepitaxial, or textured diamond films therefore is an important goal if the economical fabrication of diamond devices is to become a reality.

Heteroepitaxial or textured growth of diamond has been reported on cubic-boron nitride[7, 8], Ni[9], and Si[10-12]. Cubic-BN shows the most promise as a heteroepitaxial substrate for diamond due to its close lattice match and high surface energy. However, it is presently extremely difficult to grow c-BN in large single crystal form[13]. The recent results reported[9] of the local epitaxial growth of diamond on Ni are thus very important. Nickel has a close lattice match with diamond although its catalytic properties on the decomposition of hydrocarbons into sp^2 bonded structures, may make it difficult to inhibit the formation of graphite during diamond nucleation and growth.[14, 15] Jeng et al.[10] reported limited texturing of diamond on silicon substrates that were presumably pretreated in such a manner as to produce a semicrystalline silicon carbide surface conversion layer. However, a complete film was not formed and quantification of the amount of texture was not discussed. Other reported local epitaxy of diamond on silicon[11, 12] was most likely a limited epitaxial growth on silicon carbide as well. The lattice mismatch between β-SiC (a = 4.36 Å) and diamond (a = 3.57 Å) is rather large (~ 20%), however, β-SiC grows epitaxially on Si[16, 17] despite a 24% lattice mismatch thereby indicating that such a mismatch does not prohibit heteroepitaxy.

* Preprint of paper accepted for publication in Applied Physics Letters

In this article, the authors report the observation of textured diamond growth on (001) β-SiC substrates. The present results were obtained by a bias-pretreatment followed by standard microwave plasma CVD. The biasing pretreatment has been reported elsewhere[18, 19] and has been shown to enhance nucleation by several orders of magnitude depending on the biasing time.

II. Experimental

Samples were grown in an ASTeX microwave plasma CVD reactor (Figure 1). The power supply used was an ASTeX S-1000, 2.45 GHz microwave supply with a rectangular waveguide that is coupled to the cylindrical growth cavity. The substrate holder is a fully retractable, differentially pumped tantalum heater that may be used to control the substrate temperature independently of the plasma power. The plasma forms at a stable position in the center of the cavity and the substrate position relative to the plasma may be varied between 0(immersed) and 8 cm. The tantalum heater consists of a Ta filament encased in a boron nitride insert that fits inside of a differentially pumped, isolated 0.04 inch thick tantalum can. As shown in figure 1, the substrate holder fits onto the tantalum can, which is in turn connected to an electrical feedthrough. With this arrangement, the substrate may be biased or isolated from ground. A detailed explanation of the biasing arrangement has been published elsewhere[19].

Diamond was deposited on 1 inch diameter (001) b-SiC films that were grown epitaxially in a separate reactor on (001) Si substrates using conventional CVD techniques [16, 17, 20]. The b-SiC films (4-5 mm thick) were prepared by polishing the as grown surface with 0.1 mm diamond paste to minimize the surface roughness. The sample was then oxidized in O_2 at 1200 °C to a thickness of approximately 0.1 mm in order to remove the majority of the surface damage that occurred during the polishing. This is also expected to eliminate all carbon/hydrocarbon contamination which may have occurred during polishing. Just prior to insertion into the growth chamber, the oxide was stripped using a 10:1 mixture of HF:DI-H_2O followed by a DI rinse and drying with nitrogen.

The pretreatment and growth conditions are outlined in Table 1. The pretreatment consisted of biasing the substrate for 30 min at -250 volts while it was immersed in a 2% methane-in-hydrogen plasma. The pressure was 15 torr, microwave power 600 watts, and total flow rate was 1000 sccm. The substrate temperature was approximately 650 °C and the resulting current was 100-150 mA, collected through the substrate holder with a top surface diameter of 1.5 inches. After the 30 min pretreatment, the voltage was turned off, and the substrate was moved to a position approximately 1 cm from the edge of the glow discharge region of the plasma. The methane concentration was reduced to 0.5%, the pressure increased to 25 torr, and the temperature was maintained at 650-700 °C. These growth conditions are those which in the past have resulted in high quality diamond films with little secondary nucleation and

modest growth rates of approximately 0.05 mm/hr.

Diamond was grown on the b-SiC sample under the above condition for 10, 35, and 50 hrs and analyzed after each growth period. Scanning electron microscopy (SEM), and Raman spectroscopy were used to characterize the diamond on SiC. After the analysis, the sample was rinsed with DI water, blown dry with nitrogen and then reinserted into the chamber for continued growth. In this manner, changes in the morphology and texture of the diamond could be observed with increased deposition time.

III. Results and Discussion

Figures 2(a)-(c) show SEM micrographs taken at different locations on the sample after 50 hrs of growth. Figure 2-(a) was taken in the center, (c) near the edge, and (b) in between the two. Arrows, pointing in the SiC <110> direction show that over 50% of the diamond particles on the surface are textured with (001) faces parallel to the SiC (001) and with the diamond <110> parallel within 3° to the <110> of SiC. The micrographs also depict the nonuniformity of the diamond deposition. This was most likely due to the relatively short pretreatment time (~ 30 min). In the past, a pretreatment time of 1 to 1.5 hrs was required to achieve uniform nucleation on Si[18, 19]. A shorter time was utilized in the present study to minimize damage to the SiC surface since heteroepitaxial deposition was the objective. Figure 3 shows a schematic representation of an oriented diamond particle on the SiC wafer. Higher growth in the <110> than in the <110> has made the top (001) face rectangular rather than square. In a cubic system one should normally expect uniform growth in all the <110> directions. However preferential growth in a particular <110> direction may occur along steps, which are known to occur along the SiC<110> on the (001) surface[2, 16]. Figure 4 shows an SEM taken at 45 °, indicating that the (111) are the most stable, slowest growing planes and are therefore the largest. Reflection high energy electron diffraction(RHEED) was also performed on the sample after 10 hrs of growth. Streaks as opposed to rings were observed for the diamond (400) and (220) orientations, thus confirming that the particles were textured.

Micro-Raman Spectroscopy (Figures 5(a) & (b))was performed on the sample after 50 hrs of growth in the regions represented by SEM figures 2(a-c). The sharp 1332 cm^{-1} diamond peak[21] and the absence of the broad peak at 1500 cm^{-1} indicate that the diamond is of high quality with undetectable graphitic component. SiC peaks[22] at 796 and 973 cm^{-1} were also observed from the substrate.

Researchers have attempted to grow on single crystal SiC in the past. Hartnett et al.[23] reported three times higher growth rates on (110) textured b-SiC than on silicon but the diamond was randomly oriented. Glass et al.[24] reported that initial attempts to grow on both on-axis and off-axis b-SiC via HFCVD were unsuccessful and that surface abrasion was

necessary in order to achieve significant diamond nucleation. A U.S. patent has been awarded to Imai and Fujimori of Sumitomo Electric, Ltd., Japan[25] for the growth of single crystal diamond on GaAs via an intermediate layer of single crystal silicon carbide. This patent is encouraging, however, details of the growth process are unclear.

The present authors believe that the biasing pretreatment on SiC has played an important role in enhancing the nucleation without significantly damaging the surface so as to destroy its crystallinity. In a recent study of the bias enhanced nucleation process via in vacuo surface analysis and TEM[18], the authors observed that diamond nucleation on silicon was preceded by the formation of an interfacial carbide layer covered with a very thin (5-10 Å) non-diamond carbon film. It was also found that the biasing process removed oxide and suppressed oxide formation on the surface. Since an amorphous oxide will have obvious deleterious effects on heteroepitaxial nucleation, this oxide removal is believed to be an important factor in the promotion of the present heteroepitaxial nucleation and growth. Attempts to fully remove the oxide from both SiC and Si wafers without biasing proved unsuccessful, thus suggesting that original failures achieve the heteroepitaxial nucleation of diamond on SiC may have been in part due to the inability to remove the surface oxide. In the present study, the reduction in pretreatment time (from 1.5 in the previous study to 0.5 hrs here) was believed to have minimized the surface damage while still creating sufficient nucleation via the impingement of carbon ions from the plasma[18]. In conjunction with the oxide suppression, this has allowed the heteroepitaxial nucleation and growth of diamond on SiC in the present study.

IV. Summary

It has been shown here that textured and epitaxial diamond particles can be grown on (001) b-SiC. Based on SEM observations approximately 50% of the diamond nuclei are textured with the (001) parallel to the SiC substrate and <110> directions aligned within 3°. The nucleation was enhanced by first biasing the substrate in a 2% methane/hydrogen plasma for 30 min. This biasing pretreatment is believed to enhance the nucleation without damaging the substrate thus allowing limited heteroepitaxial growth.

Acknowledgement

The authors wish to thank X.H. Wang and R.J. Nemanich for performing the Raman spectroscopy, and M. Paisley, Y.C. Wang and R.F. Davis for providing the SiC substrates and valuable technical assistance. Valuable discussions with G.H. Ma of NCSU, and D.L. Dreifus and W. Hooke of Kobe Steel, EMC are also greatly appreciated. This research was financially supported in part by SDIO/IST through ONR and the Kobe Steel, Ltd. Professorship at NCSU.

References

1. R. F. Davis, International Journal of Materials & Product Technology, 81 (1989).
2. R. F. Davis and J. T. Glass, "The Growth and Characterization of Silicon Carbide and Diamond for Microelectronic Applications," in *Advances in Solid-State Chemistry*, edited by JAI Press Ltd., p. 1 (1991).
3. S. Kurita, Japan New Diamond Forum, 113 (1990).
4. M. N. Yoder, *First International Conf. on the Applications of Diamond Films and Related Materials, Auburn, Alabama, U.S.A., Aug. 17-22, 1991*, edited by Y. Tzeng, M. Yoshikawa, M. Murakawa and A. Feldman, Elsevier, p. 287 (1991).
5. M. Seal, *First International Conf. on the Applications of Diamond Films and Related Materials, Auburn, Alabama, U.S.A., Aug. 17-22, 1991*, edited by Y. Tzeng, M. Yoshikawa, M. Murakawa and A. Feldman, Elsevier, p. 3 (1991).
6. W. A. Yarbrough and R. Messier, Science, **39**(1), 1 (1989).
7. M. Yoshikawa, et al., Appl. Phys. Lett., **57**(5), 428 (1990).
8. S. Koizumi, T. Murakami, T. Inuzuka and K. Suzuki, Appl. Phys. Lett., **57**(563 (1990).
9. Y. Sato, et al., *Second International Conference on New Diamond Science and Technology, Washington, D.C., Sept. 23-27, 1990.*, edited by R. Messier, J. T. Glass, J. E. Butler and R. Roy, p. 371 (1991).
10. D. G. Jeng, H. S. Tuan, R. F. Salat and G. J. Fricano, Appl. Phys. Lett., **56**(20), 1968 (1990).
11. J. Narayan, et al., Appl. Phys. Lett., **53**(19), 1823 (1988).
12. B. E. Williams and J. T. Glass, J. Mater. Res., **4**(2), 373 (1989).
13. W. A. Yarbrough, J. Vac. Sci. Technol. A, **9**(3), 1145 (1991).
14. T. P. Hilditch, *Catalytic Processes in Applied Chemistry*, Chapman & Hall LTD, (1929).
15. D. N. Belton and S. J. Schmieg, J. Appl. Phys., **66**(9), 4223 (1989).
16. C. H. Carter, R. F. Davis and S. R. Nutt, J. Mater. Res., **1**(6), 811 (1986).
17. H. S. Kong, Y. C. Wang, J. T. Glass and R. F. Davis, J. Mater. Res., **3**(3), 521 (1988).
18. B. R. Stoner, G.-H. M. Ma, S. D. Wolter and J. T. Glass, Phys. Rev. B, to be submitted (1991).
19. B. R. Stoner, et al., Accepted for Publication in J. Mater. Res., submitted (1991).
20. J. T. Glass, Y. C. Wang, H. S. Kong and R. F. Davis, *Mat. Res. Soc. Symp.*, edited by p. 337 (1988).
21. R. E. Shroder, R. J. Nemanich and J. T. Glass, Phys. Rev. B, **41**(6), 3738 (1990).
22. D. Olego, M. Cardona and P. Vogl, Phys. Rev. B, **25**(3878 (1982).
23. T. Hartnett, et al., J. Vac. Sci. & Technol. A, **8**(3), 2129 (1990).
24. J. T. Glass, et al., SDIO/IST-ONR Diamond Technology Initiative Symp., Crystal City, Va. Paper T23, (1988).
25. T. Imai and N. Fujimori, United States Patent No. 4,863,529 (1989).

Table 1

Parameter	Pretreatment	Growth
CH_4/H_2 (%)	2 %	0.5%
Flow Rate (sccm)	1000	1000
Net Power (watts)	550	600
Pressure (torr)	15	25
Distance from Plasma (cm)	immersed	1 cm
Substrate Temperature (°C)	650	650-700
Bias Voltage (V)	-250	floating
Current (mA)	100-150	
Time (hrs)	0.5	10, 35, 50

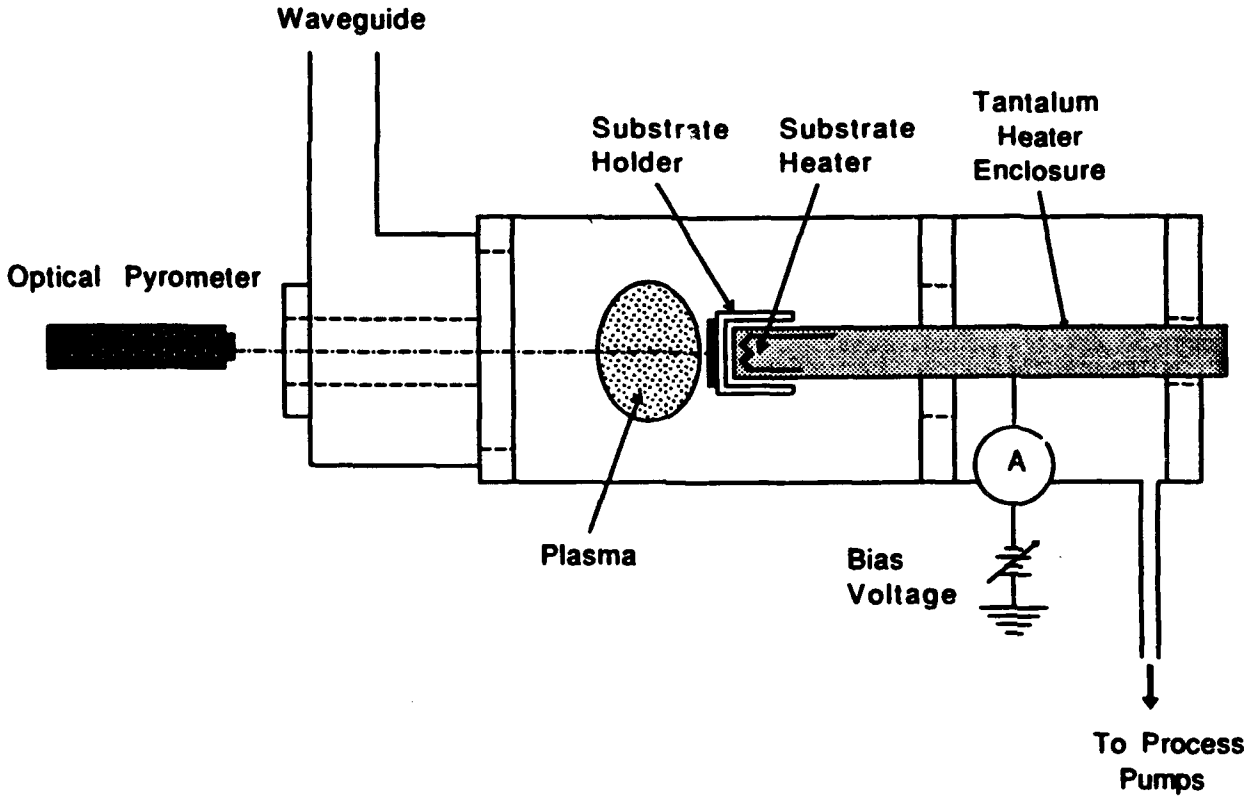

Figure 1. CVD chamber showing substrate heater and biasing arrangement.

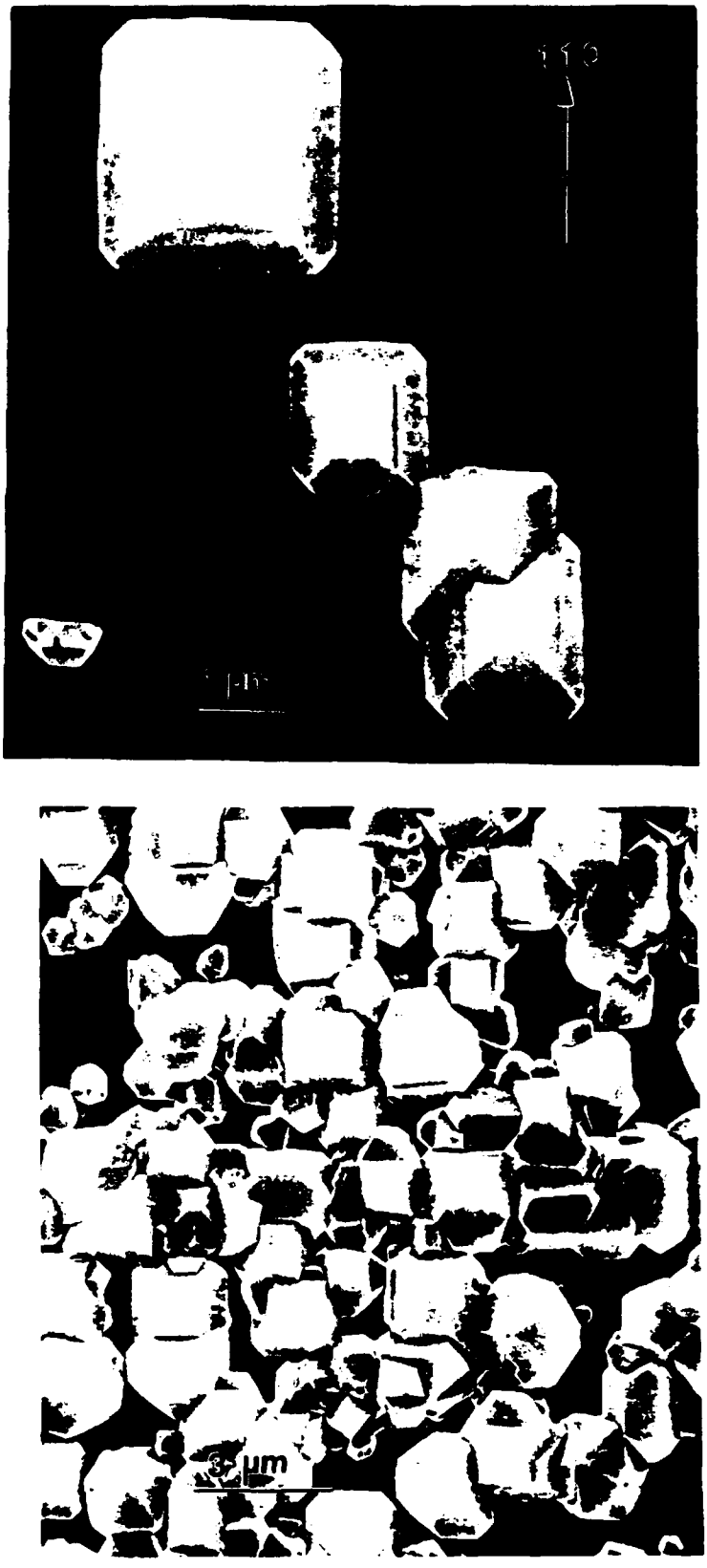

Figure 2. SEM micrographs of the textured diamond film at (a) the center region , (b) middle, and (c) edge of the sample.

Figure 2(c)

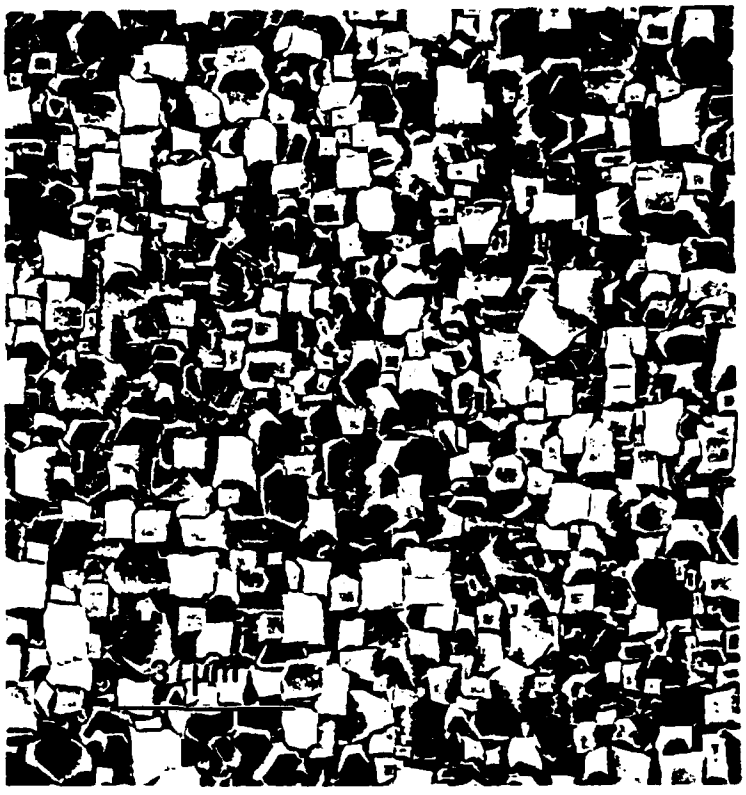

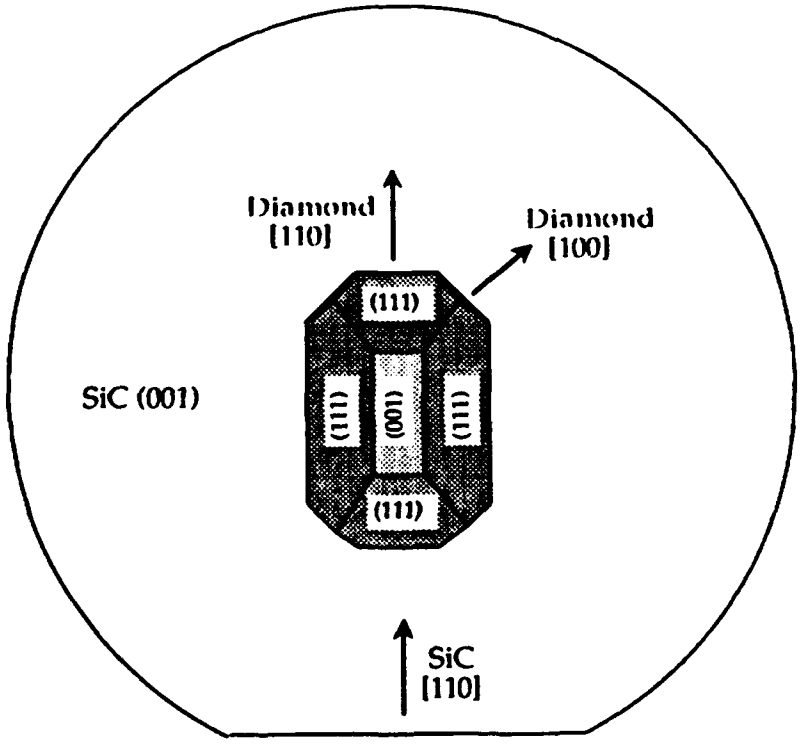

Figure 3. Schematic representation of the diamond particle orientation relative to the SiC substrate.

Figure 4. SEM of center region taken at 45 deg. tilt to show (111) faceting.

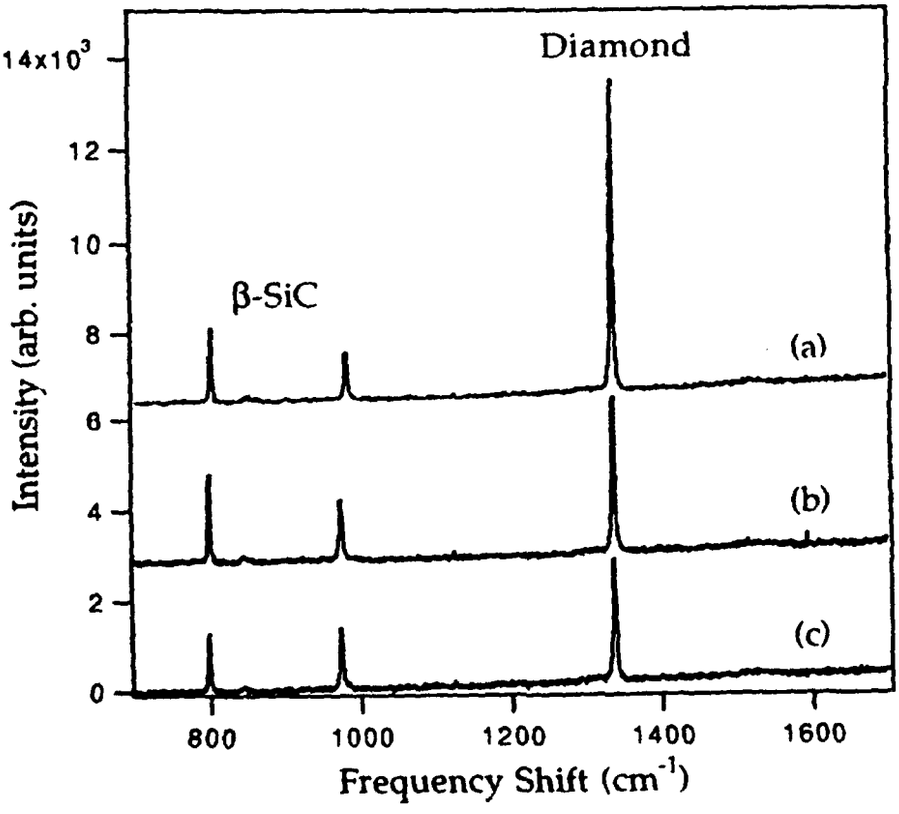

Figure 5. Micro-Raman spectra taken from the (a) center, (b) middle, and (c) edge regions of the sample.

V. OPTICAL AND SCANNING TUNNELING MICROSCOPY CHARACTERIZATION OF MICROSTRUCTURES, DEFECTS AND DOMAIN SIZE EFFECTS IN DIAMOND FILMS

A. Introduction

The properties of diamond that are often noted are hardness, resistance to chemicals, optical and X-ray transparency, high thermal conductivity, doping and high electronic mobilities. Examples of applications which utilize these properties include optical coatings, X-ray windows, hard coatings on machine tools, heat sinks and high temperature electronics. For most of these applications the microstructure and defects of the films is important. For optical coatings, microstructure of the same dimension as the wavelength will cause strong scattering. For hard coatings, microstructure can contribute to fracture, and for chemically inert applications, the internal microstructure can lead to paths of molecular diffusion. For heat sink applications the microstructure will contribute to phonon scattering which can reduce the thermal conductivity, and similarly, for electronic applications the microstructure can reduce the carrier mobility through electron scattering and recombination.

Diamond films exhibit the additional complication that the atomic bonding can have regions of graphite-like or sp^2 bonding configurations. An important aspect of the sp^2 bonded regions is that the optical and electrical characteristics of these regions are significantly different from those of diamond. Raman scattering at ~1332 cm^{-1} has proved to be an indication of diamond, while structures with center frequencies ranging from ~1350 to 1600 cm^{-1} are attributed to sp^2 bonded carbon. In addition to the difference in vibrational frequencies, the sp^2 bonded regions will be optically absorbing. The optical absorption differences of the diamond and sp^2 domains in the samples will affect the observed Raman results.[2] From the figure it is clear that the observed Raman ratio cannot be directly related to the sp^3/sp^2 ratio unless the domain size is known.

In this report, the issues related to Raman scattering characterization of the microstructure of diamond thin films are described. The dependence of the Raman spectra on the microcrystalline size is presented. The comparison is made with crystalline Si, and the results are applied to a series a diamond films. Then the Raman scattering, photoluminescence and STM from the initial stages of diamond film growth are described.

B. Experimental

Raman scattering measurements were carried out with both macro and micro-focussed laser beam excitation. To assure accurate comparisons, all spectra were excited with the 514.5nm line of an Ar ion laser for all measurements. The scattered light was dispersed with a U1000 ISA double spectrometer. In the macro-focussed configuration the laser beam was focussed to

a line image of ~2 x 0.1mm. The extended image on the sample reduced beam heating effects and allowed accurate determination of peak positions and linewidth. For the micro-focussed experiments, the beam was directed into an Olympus microscope coupled to the optical spectrometer. A spot size of ~3μm dia. could be achieved. Micro- and macro-photoluminescence measurements were obtained with the same experimental configurations. In these experiments the scans ranged over 7000cm^{-1} from the laser line which allowed detection of the 1.68 eV peak associated with defect structures in diamond films.

All STM measurements were performed with "in air" scanning systems. Two systems were used: 1) an RHK ATM-500 and 2) a Park Scientific, STM. The scans of the surface covered between 10 to 8000Å in the x or y direction. The noise levels for tunneling limited the "z-direction" resolution to ~4Å. All of the scans were performed with tunneling currents ranging between 0.2nA to 0.3nA. The tip bias was between ± 5V. For boron doped films, high quality images were obtained in both bias polarities. For the undoped films higher quality images were obtained with the tip biased at -2V with respect to the sample.

The Park Scientific system was used to obtain I-V measurements at points on the surface. These techniques are termed scanning tunneling spectroscopy. The system allowed several different averaging methods to obtain I-V spectra and average the results.

C. Results and Discussion

1. Domain Size Dependence

While the domain size dependence of the Raman spectrum of graphite has been well studied, similar effects have only recently been considered for diamond.[4,5] The models which describe the effects due to microcrystalline domain size have been established originally in studies of BN [6] and Si.[7,8]

For Raman scattering from single crystal material, sharp features are observed which are due to the vibrations of the crystal. For the diamond lattice (or Si), a single mode is selected from the spectrum of all of the vibrational modes of the crystal. The single mode that is observed is determined from the wavevector (or momentum) selection rules which apply to the Raman scattering process. In contrast, for scattering from amorphous materials, the Raman spectrum is continuous and often is similar to the vibrational density of states of the material. This is because the vibrational states do not have well defined wavevector, and the wavevector selection rules are totally relaxed.

For microcrystalline samples, the wavevector selection rules are partially relaxed due to the uncertainty of the wavevector. The uncertainty is determined by the Heisenberg uncertainty relation

$$\Delta q \, \Delta x \geq 2\pi$$

where Δq is the wavevector uncertainty and Δx is the size of the crystal. The complete analysis for a particular crystal requires determination of the scattering structure factor for scattering from all the modes in the crystal. [6-8]

The model is briefly summarized here.[8] We make the assumption that the dispersion curves are not changed nor are there any new modes created for the microcrystalline domains. The phonon excited in the lattice by the incident photon is confined to the microcrystallite in which it originates. We also assume that the scattering geometry selects the q=0 vibrational mode. While this is not the case in general, the actual wavevector selected by the scattering geometry will be $\sim 2\pi/\lambda$ where λ is the laser wavelength, typically 500nm. This will be small compared to the wavevector uncertainty ($2\pi/l$) for $l < 100$nm. The phonon confinement function that characterizes the wavevector uncertainty is usually taken to be a Gaussian of the form

$$|C(0, q)|^2 \equiv \exp(-q^2L^2/16\pi^2),$$

where L is the diameter of the sphere in which the phonon is confined and C(0, q) are the Fourier coefficients for first order Raman scattering ($q_o = 0$). This representation is simply a restatement of the Heisenberg uncertainty relation noted above. Given these coefficients it is possible to calculate the Raman spectrum I(ω):

$$I(\omega) = \int \frac{d^3q|C(0,q)|^2}{[\omega - \omega(q)]^2 + (\Gamma_o/2)^2},$$

where $\omega(q)$ is the full set of the phonon dispersion relations of the crystal and Γ_o is the natural linewidth. This integration must be performed over the complete Brillioun zone. In general, if L does not become too small, i.e. L > 30 Å we can still focus on a small region around the center of the Brillioun zone. If a numerical calculation is carried out from the above equation, it is found that not only does the peak frequency shift as the crystalline domain size decreases, but also the peak width (FWHM) increases. If the branch of the phonon dispersion curve of interest is a decreasing function of q (the wavevector), then the average scattered phonon will have a lower frequency than a phonon scattered in an infinite crystal. This is the case for Si and because of this the Raman peak will exhibit a smaller Raman shift. The calculation has been carried out by Fauchet and Campbell,[8] and the relation of the peak frequency and FWHM

to the domain size is illustrated graphically in Figure 1. Experimental results have verified this relation for Si.

Because the crystal structure of silicon resembles that of diamond, we suggest that the above analysis should be applicable to diamond.[4] Since this analysis relies only on the shape of the phonon dispersion curves of silicon, these curves were compared to those of diamond. The dispersion curves of both materials along the (011) direction are shown in Figure 2.[9,10] It is obvious from this figure that the curves in this wavevector direction are similar in shape. By examining the region around Γ=0 (the region sampled in the Raman scattering event), it is seen that both dispersion curves can be approximated with straight lines. In order to determine the multiplicative factor to be used in the calculation for diamond, the ratio of the slope of the dispersion curve along this line was calculated from the graph. This value was then corrected for the reduced wavevector and it was determined that the average slope of the curves agree within the experimental accuracy of ± 2%. Therefore the results obtained for Si can be used exactly for diamond.

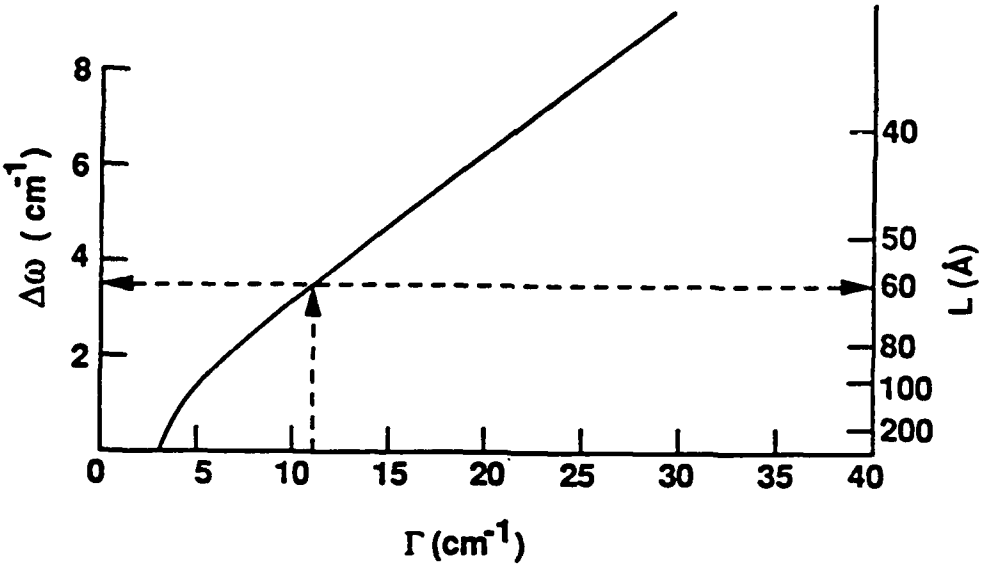

Figure 1 The relation of microcrystalline domain size to linewidth, Γ, and peak shift deduced for Si and applied to diamond. The dashed line represents the example described in the text.[8]

The spectra of diamond microcrystals was previously reported by Solin and Kobliska,[11] and their results indicated a linewidth of 14 cm^{-1}. The analysis presented above would indicate an average domain size of 73Å. This is consistent with the reported 40 to 100Å domain size of the powders.[11]

To illustrate the microcrystalline effects, a series of diamond films was analyzed with this model. The samples were grown in an rf plasma CVD system and the pressure was varied from 1 to 10 torr for the depositions.[4] The Raman spectra are shown in Figure 3, while Table 1 gives the linewidth (FWHM) calculated from the spectra along with the domain size corresponding to this linewidth.

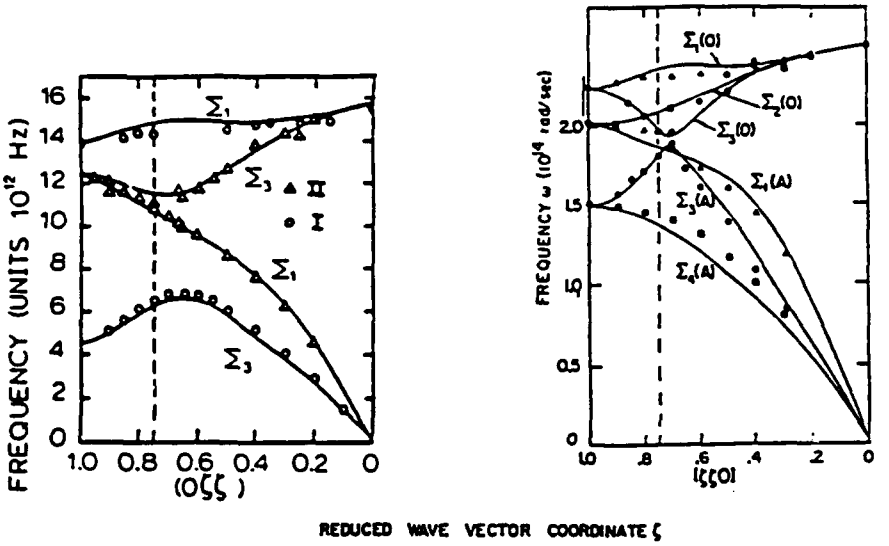

Figure 2. *The phonon dispersion relations for diamond and Si for wavevectors along the* (100) direction (from refs. 9 and 10).

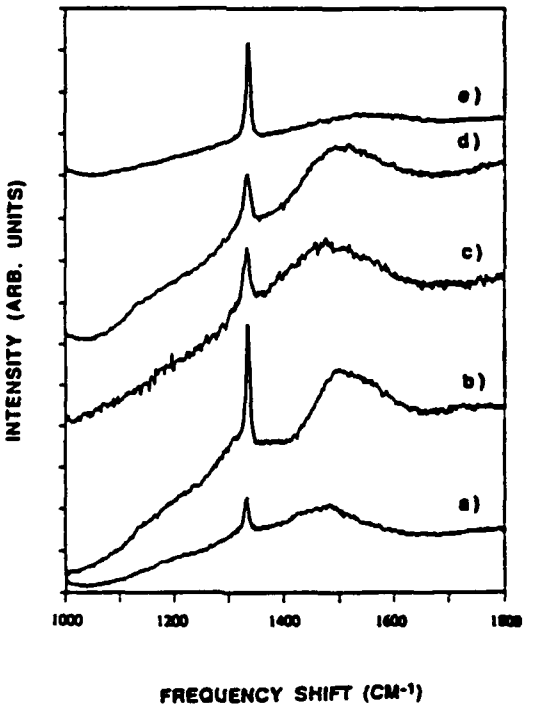

Figure 3. The Raman spectra of a series of diamond films grown be rf-plasma CVD. The different films were obtained at different pressures.[4]

Table I. The observed linewidth and deduced domain sizes for the series of CVD diamond films grown at different pressures.

Pressure (torr)	Linewidth (cm^{-1})	Domain size (Å)
1	9.6	70
3	6.2	98
5	13.5	57
7	11.3	60
10	8.7	78

An example of the method used to deduce the domain size is illustrated in the Fig. 1. For an observed Raman peak width of 11 cm^{-1}, from the graph, a crystalline domain size of ~60 Å is deduced. Because aspects such as strain and relative isotope can also contribute to the observed Raman frequency, it is probably more reliable to base the analysis on the peak width rather than on peak position.

It should be noted that scanning electron microscopy (SEM) pictures of these films showed crystallite sizes varying from .5 to 2.5μm, which is much larger than that determined from our analysis. Previous research has shown that the domain size calculated from Raman scattering and grain sizes measured from TEM and SEM are generally inconsistent, with these microscopy techniques yielding larger values than Raman scattering.[12] However, electrical and thermal conductivity measurements may be in agreement with those obtained by Raman. Thus it is implied that the actual order of the particles is limited by microstructure within the particles. The presence of twins, stacking faults and dislocations have been identified in TEM examinations of the films,[12] and it is likely that these structures will lead to limited wavevector correlation and to phonon and electron scattering.

2. Microstructures of the initial stages of growth

One of the most critical aspects of diamond film growth is the nucleation process. For most diamond growth methods, it is necessary to polish or roughen the substrate surface to obtain reasonable nucleation rates. Even when this procedure is utilized, It usually requires a deposition time of ~3hrs to achieve complete coverage for microwave plasma CVD or hot filament CVD. Obtaining a Raman signal from films with incomplete coverage will require micro-focussing on the diamond nuclei.

We have recently carried out a series of measurements on the initial stages of microwave CVD diamond growth on Si substrates.[13,14] Films were prepared with 60 min. exposure to the same conditions used to grow high quality diamond. An SEM examination of the films

showed very sparse nuclei of ~0.25μm. The surfaces were then examined by scanning tunneling microscopy (STM), micro-Raman, micro-photoluminescence and surface enhanced Raman scattering.

The STM image shown in Fig. 4 displays a nuclei that has formed on the surface. The nuclei has formed at the intersection of two scratches. In addition, the other regions of the surface displayed roughening or growth. The STM measurements showed that the surface of the nuclei is flat and is parallel to the substrate to within 5°. It is interesting to note that while the nucleation apparently occurred in the groove of the scratch, the growth of the nuclei is affected by the substrate surface.

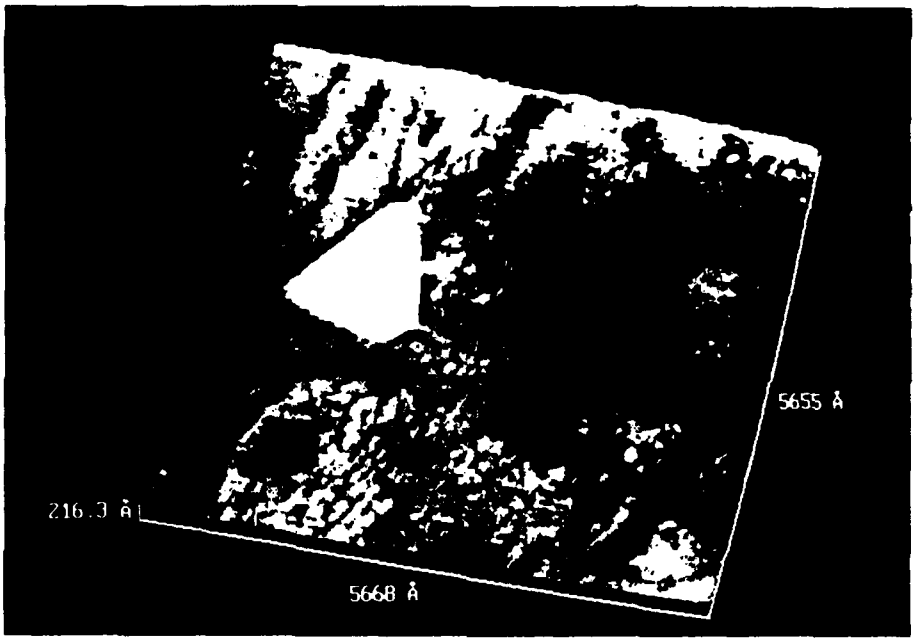

Figure 4. A scanning tunneling microscope image of a nuclei on a Si surface after exposure to microwave plasma CVD growth conditions for 60 min.

To confirm that the nuclei represented diamond growth, micro-Raman measurements were carried out, and the results are shown in Fig. 5. The micro-Raman measurements were carried out with an ISA U1000 double monochromator equipped with a microfocussing stage. It is estimated that the laser spot size on the sample surface was ~2μm. To obtain spectra from the nuclei, it was necessary to find a region on the sample with several (~10) nuclei in the laser spot. Micro-Raman measurements were obtained from regions where there were few (<3) nuclei, and the results are shown in Fig. 5. It is clear from these results that the nuclei are diamond. The observed linewidth of the nuclei is ~11cm^{-1}. This is considerably larger than the (~7cm^{-1}) linewidth that is obtained from thicker films grown under the same conditions.

Thus it can be concluded that the initial nuclei exhibit increased microstructural defects from the thicker films grown under the same conditions.

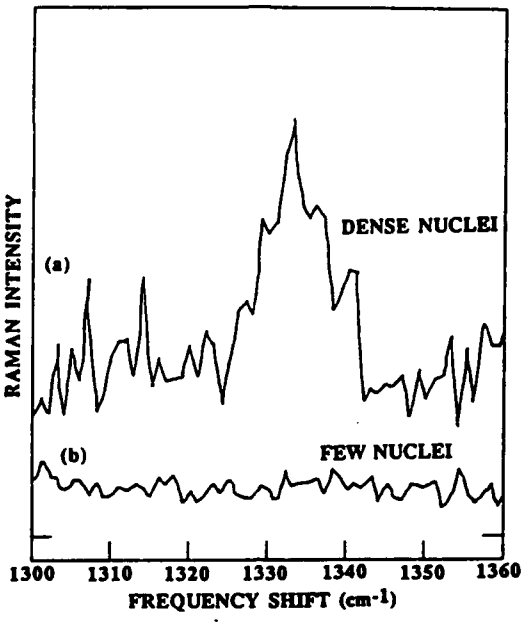

Figure 5. Micro-Raman of the initial stages of microwave CVD diamond growth. The spectra were obtained from the same sample used to obtain the STM image shown in Fig. 4.

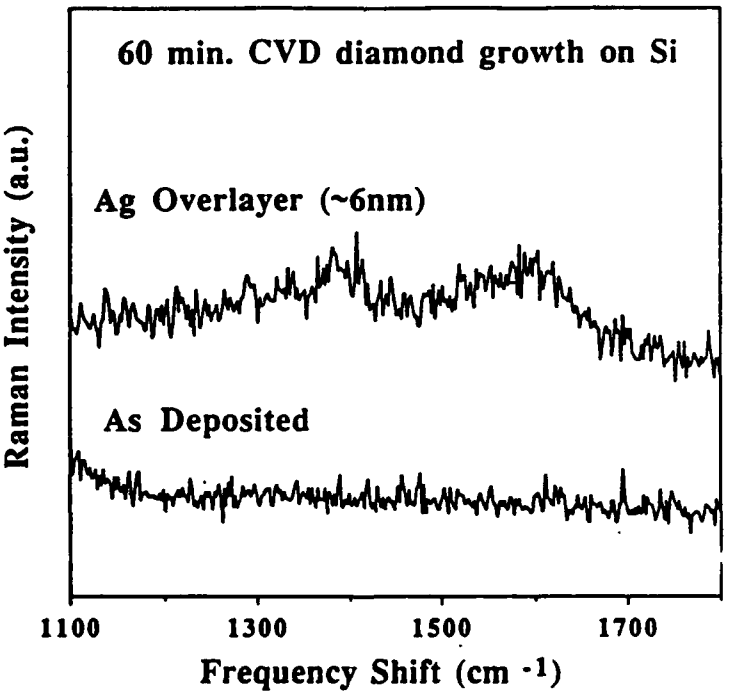

Figure 6. Surface enhanced macro-Raman scattering of the initial stages of microwave CVD diamond growth. The spectra were obtained from regions of the sample which had a 6nm layer of silver and from regions with no silver deposition.

The Raman measurements indicate that there is no diamond in the regions between the nuclei. To explore this further we initiated surface enhanced Raman scattering measurements following the recent results of Knight et al.[15] In these experiments it was found that deposition of a thin layer of silver on the surface enhanced the Raman scattering from the film. A 6nm layer of silver was sputter deposited onto the same sample used in the STM and micro-Raman studies. In this case the measurements were obtained with macro-focussing, and the results of are shown in Fig. 6. Without the silver, there was no evidence of any structure for the very thin film growth. We note that there was no signal observed from the regions between the diamond nuclei with the micro-Raman measurements. With the silver, however, a signal is observed with two features at frequencies similar to that obtained from microcrystalline graphite. Thus it appears that there is a component of microcrystalline graphite on the surface region. We also attempted to determine whether there was any evidence of SiC on the surface, however, the spectral region where these features would occur were masked by a strong signal from the Si substrate.

Diamond films also show photoluminescence which can be observed with the same experimental apparatus as the Raman spectra. The spectra are obtained by simply scanning to longer wavelength. Thus micro-photoluminescence spectra can be obtained from the same regions as the micro Raman and the results are summarized in Fig. 7. The region of dense nuclei shows a spectrum similar to that observed from thick films while the region of sparse nuclei shows no detectable signal.

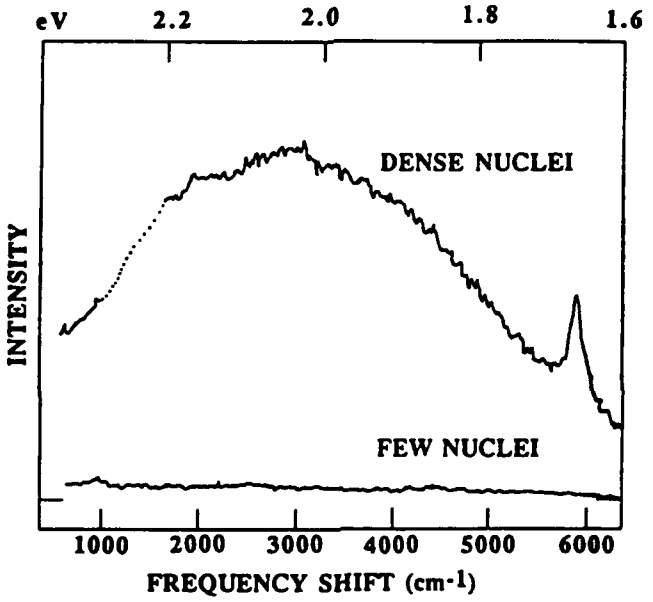

Figure 7. The micro-photoluminescence spectra of the same two regions described in Fig. 9.

The micro-photoluminescence signal of the 0.25μm nuclei has two clearly observable features: a broad feature centered at ~2.0 ev and a relatively sharp feature at 1.68 eV. The origin of both is still being explored. Possibilities for the ~2.0 eV feature include that it is due to N impurities or that it is non-thermalized emission. The 1.68 eV line is often assigned to the GR1 line observed in natural diamond which has been attributed to a charge neutral C vacancy. An alternative explanation is that it is due to Si impurities or possibly as a Si-vacancy complex. [15]

Micro-photoluminescence measurements have also been obtained from thicker samples grown under the same deposition conditions. The spectral shape of the ~2.0eV line is essentially the same as the initial nuclei. In contrast, the relative intensity of the 1.68eV line is found to be much weaker. These results could be consistent with the model that the 1.68eV line is due to Si impurities which are more prevalent at the initial stages of deposition. The Si impurities could be incorporated by diffusion from the substrate or by incorporation due to H reaction with the exposed substrate. It is well established that atomic H exposure of Si results in etching, and the etched material could be incorporated in the growth surface. A higher Si incorporation rate during initial growth would be anticipated for both mechanism. Further research on both the origin of the photoluminescence and the relation to growth conditions are necessary to fully understand these results.

The current-voltage characteristics of the individual nuclei and the substrates were determined by preforming current imaging tunneling spectroscopy (CITS). In this process, an I-V curve is taken at each point in the scan. The I-V spectra taken over the nuclei were averaged and the curves taken over the substrate were also averaged together. For both the doped and undoped samples, the I-V response of the nuclei were essentially the same with only slight differences for negative voltages. The regions between the nuclei had a greater current response than the nuclei. Previous studies have shown that a layer of SiC and/or a sp^2 carbon layer is deposited on the substrate during diamond deposition. For positive bias voltages a "turn-on" of ~ 0.75 volts was observed for the regions between the nuclei of both the doped and the undoped samples. For negative biases, characteristics of negative differential resistance (NDR) were observed.

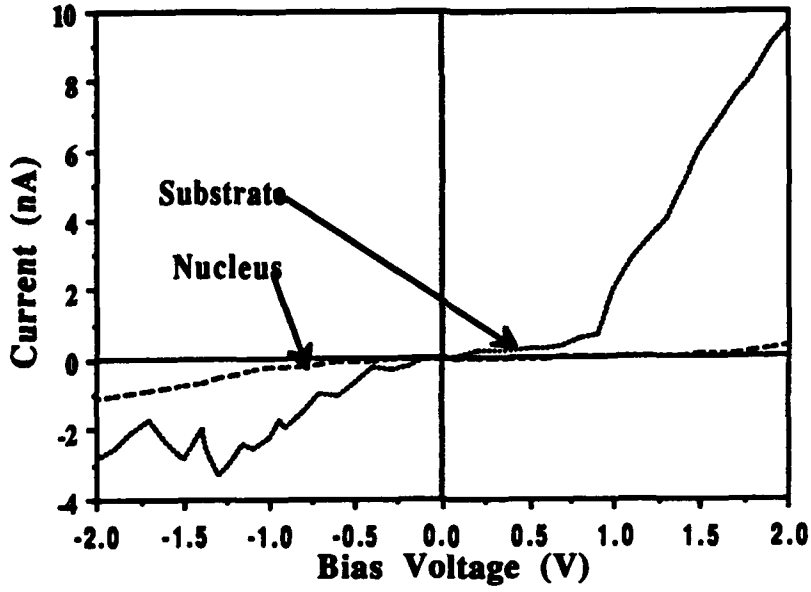

Figure 1 - Current-Voltage spectra of the nuclei and the areas around the nuclei for an undoped sample.

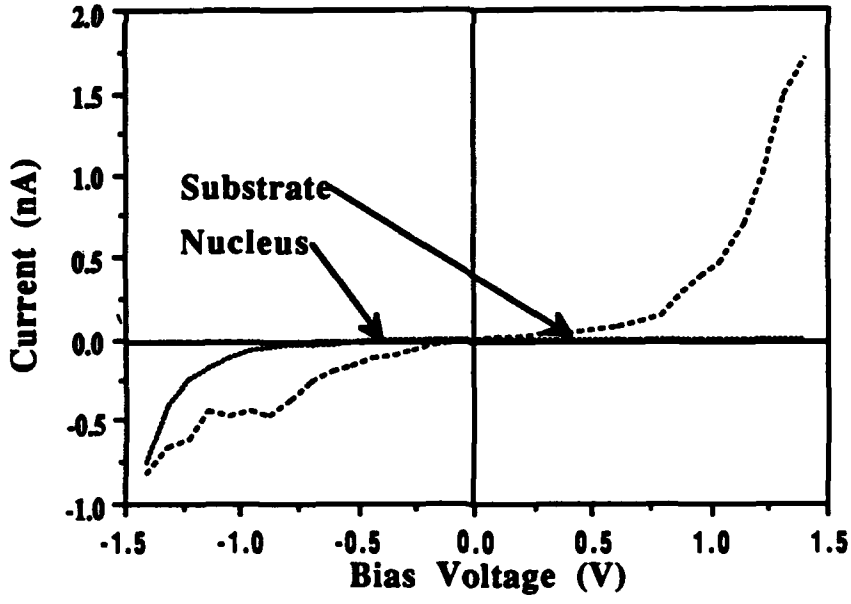

Figure 2 - Current-Voltage spectra of the nuclei and the areas around the nuclei for a doped sample

D. Conclusions

While there are many opportunities for the application of diamond thin films, many of these will be dependent on improved microstructure. Two aspects of the microstructure considered

here are regions of sp^2 bonding and diamond domains. Raman scattering can prove useful in characterizing both of these aspects. The analysis presented here was applied to a series of diamond films grown under different conditions, and this resulted in differences in the diamond domain size. Diamond nuclei were observed and microcrystalline graphite regions were detected by surface enhanced Raman scattering. The microstructure during the initial stages of diamond growth was correlated with STM images. The morphology of doped and undoped diamond nuclei appear to be similar. The I-V spectra for both doped and undoped diamond exhibit similar aspects. In both cases the spectra were distinct from the substrate which exhibited ohmic characteristics.

E. Future Research Plans

1. Nucleation on Dissimilar Substrates

The growth of large single crystal diamond requires the formation of oriented diamond nuclei. Furthermore, it has been well established that nucleation is affected by the substrate morphology (ie polishing with diamond grit). We will emphasize Scanning Tunneling Microscopy and Spectroscopy (STM and STS) to study the initial substrate interactions and nucleation processes. Micro-Raman scattering and micro-photoluminescence will also be used to characterize the bonding structure and defects. Initial studies will focus on measuring the properties of the different growth processes while further studies will focus on changes due to different substrates such as vicinal surfaces.

While STM from insulating samples is difficult and impossible in some cases, the technique will be directly applicable to studies of the initial nucleation process because conducting Si substrates often used for diamond film growth have proven to be well characterized with STM. We were the first group to demonstrated the use of STM on doped CVD diamond thin film. In addition we have recently demonstrated very high quality images from small nuclei of undoped films on Si substrates.

The interface structure and electronic properties will play an important role in device structures, and may also play a role in the nucleation of the films. For the Si/Diamond interface, it will be important to determine the heterojunction band offset. A new method to determine the band offsets or Schottky barrier is ballistic electron emission spectroscopy or BEEM. To accomplish this two approaches will be employed- (1) epitaxial Si films will be deposited on diamond, and (2) diamond films deposited on Si will be thinned by etching. The measurements will probably require BEEM - hole measurements and this effect has recently been demonstrated.

There is significant evidence that natural diamond substrates are unsuitable for device applications because of extended defect structures and crystalline mosaic. We will also explore

the role of surface mosaic and structure in the homoepitaxial growth process. This will be accomplished by depth profile micro-Raman and cathodo-luminescence.

2. Growth Induced Defect Structures

The structure of the films is often determined by the processes that occur at the growth surface. For diamond the processes are complicated because of the gas-surface reactions and the competition between formation of sp^2 bonded structures and etching of sp^3 bonded structures. In addition, electronic device applications require doping and p-type doping has been demonstrated with boron. While n-type doping has been reported for several different processes including Li incorporation, the processes have not been fully characterized and different groups have had difficulty repeating the experiments. An aspect that often limits the dopant properties is the formation of dopant-impurity-defect complexes.

We have developed a series of experimental characterization techniques which can address the structure and electronic properties of surfaces. These include STM and related STS and BEEM, angle resolved photoemission, depth profile cathodo-luminescence, micro-photo-luminescence and micro-Raman.

Recent studies have suggested that the growth surface involves sp^2 bonded carbon structures, and there have been many suggestions for the surface interactions which lead to diamond film growth. The growth must then involve a transition to sp^3 bonding to form the diamond lattice. The transition may be strongly affected by the presence of H, O or a halogen. To explore this effect, surface characterization measurements will be employed to examine the surface immediately after stopping the growth. The growth stoppage must occur without H exposure which could etch or assist in removal of the structures present during the growth. We have already observed significant effects in the micro-Raman from polycrystalline films grown identically but with different shutdown procedures. These experiments must be repeated with homoepitaxial films on (111) and (100) oriented substrates. In addition, we will employ the other surface sensitive techniques. In particular, STM and related STS. The STM will observe the atomic scale structure, and the STS technique can identify the local density of electron states on the surface.

The incorporation of dopants and the role of defects and impurities will also be examined with the surface spectroscopies. We will examine a series of samples produced with different levels of impurities. The first impurities that will be explored are N, O, and Si. These studies are in progress and several photo-luminescence transitions have been observed. Since device structures will almost certainly involve dopant incorporation in homoepitaxial films, we will study these effects with homoepitaxial films on diamond substrates (B, Li). Again we will apply STM and STS techniques with a goal of identifying whether the dopants are uniformly incorporated or clustered at or on the surface. In addition, we have recently developed a

method of obtaining depth sensitive cathodo-luminescence measurements. The cathodo-luminescence will be excited in UHV using an electron gun with a fine controlled energy range from 3000eV down to 40eV. Over this energy range the electron penetration is from 50Å to less than 15Å. The cathodo-luminescence excited with different electron energies will reflect the bulk or surface contributions. We have recently observed the cathodo-luminescence visually from this system and we are in the process of installing a spectrometer to record the spectrum.

F. References

1. R. J. Nemanich, J. T. Glass, G. Lucovsky, and R. E. Shroder, J. Vac. Sci. Technol. **A6**, 1783 (1988).
2. R. E. Shroder, R. J. Nemanich, and J. T. Glass, Phys. Rev. **B41**, 3738 (1990).
3. F. Tuinsta and J. L. Koenig, J. Chem. Phys. **53**, 1126 (1970).
4. Y. M. LeGrice, R. J. Nemanich, J. T. Glass, Y. H. Lee, R. A. Rudder, and R. J. Markunas, Mat. Res. Soc. Symp. **162**, 219 (1990).
5. R. J. Nemanich, E. C. Buehler, Y. M. LeGrice, R. E. Shroder, G. N. Parsons, C. Wang, G. Lucovsky, and J. B. Boyce, Mat. Res. Soc. Symp. **164**, 265 (1990).
6. R. J. Nemanich, S. A. Solin, and R. M. Martin, Phys. Rev. **B23**, 6348 (1981).
7. H. Richter, Z. P. Wang, and L. Ley, Solid State Commun. **39**, 625 (1981).
8. P. M. Fauchet and I. H. Campbell, Critical Reviews in Solid State and Materials Sciences **14**, S79 (1988).
9. P. A. Temple, and C. E. Hathaway, Phys. Rev. B **7**, 3685 (1973).
10. S.A. Solin, and A. K. Ramdas, Phys. Rev. B **1**, 1687 (1970).
11. S. A. Solin and R. J. Kobliska, in Amorphous and Liquid Semiconductors, edited by J. Stuke (Taylor and Francis, London, 1974), p. 1251.
12. B.E. Williams and J.T. Glass, J. Mater. Res. **4**, 373 (1989).
13. K. F. Turner, B.R. Stoner, L. Bergman, J.T. Glass and R.J. Nemanich, proc. of the 2nd Int. Conf. on the New Diamond Science and Technology, (Mat. Res. Soc., Pittsburgh, 1990) in press.
14. R.J. Nemanich, L. Bergman, Y.M. LeGrice, and R.E. Shroder, proc. of the 2nd Int. Conf. on the New Diamond Science and Technology, (Mat. Res. Soc., Pittsburgh, 1990) in press.
15. D.S. Knight, R. Welmer, L. Pilione, and W.B. White, Appl. Phys. Lett. **56**, 1320 (1990).

VI. Interface Reactions of Titanium on Single Crystal and Thin Film Diamond

A. Introduction

Along with the rapidly advancing field of CVD diamond thin films for electronic applications, there is an increased interest in metal contacts on diamond. These contacts can be either ohmic or rectifying, depending on the metal, surface preparation prior to metal deposition and treatment of the contact [1].

Previous studies by the investigators have shown that heteroepitaxial nickel films can be successfully grown on natural C(001) substrates by thermal and electron-beam evaporation [2,3]. In particular, *in situ* LEED and Auger electron spectroscopy techniques were used to investigate the surface structure and determine the corresponding growth modes for the nickel overlayer. Moreover, both SEM and STM techniques were employed to examine the surface topography and determine the degree of surface roughness. Furthermore, it has been demonstrated from RBS/channeling measurements that the Ni/C(001) interface is both physically and chemically abrupt. In addition, as evidenced by current-voltage characteristics the as-deposited nickel films exhibit stable rectifying properties in the 25-400^{o}C temperature range. Subsequent post-growth annealing studies at 1100^{o}C were also implemented to investigate the thermal and chemically stability of the Ni contacts.

Titanium is known to form a Schottky contact on diamond when deposited at low temperatures but is generally used to form an ohmic contact by annealing the contact above 580°C [4,5], or by depositing the titanium while the diamond is kept at 400°C [6]. The transition from rectifying behavior to ohmic behavior after annealing has been shown for other carbide forming metals [4]. In this study we have employed angle resolved uv-photoemission spectroscopy, (ARUPS), to observed the onset of titanium carbide formation for UHV deposited titanium films on both single crystal diamond and diamond thin film.

Although there have been many reports of the rectifying behavior of titanium on diamond, to our knowledge no measurements of the Schottky barrier height have been reported. Due to the high ideality factor of the titanium-diamond rectifying contact it is generally difficult to determine the Schottky barrier height using I-V measurements. The position of the valence band maximum on the surface of diamond relative to the Fermi level of a titanium film can be determined from the ARUPS data. The energy difference is the Schottky barrier height for the metal on a p-type semiconductor. This technique was used to determine the Schottky barrier height for UHV deposited titanium on both diamond thin film and single crystal, type IIB, diamond with a (111) orientation.

B. Experimental

The ARUPS data was measured with a 50mm hemispherical analyzer with an ultimate energy resolution of 0.02eV and an angular resolution of 2°. The analyzer is mounted on a two stage goniometer which allows angle dependent measurements. As an excitation source a differentially pumped helium discharge lamp was used, which generated HeI (21.2eV) radiation. The base pressure of the ARUPS chamber was $<1 \times 10^{-9}$ Torr with an operating pressure of 5×10^{-9} Torr. The sample was mounted on a heating stage which allows the samples to be annealed up to ~1000°C. The ARUPS chamber is equipped with a Ti-filament deposition source. The pressure during deposition was $\sim 5 \times 10^{-8}$ Torr which dropped rapidly after the filament was turned off. The samples can be transferred from the ARUPS chamber under UHV conditions into a rf-plasma chamber. Both argon and hydrogen plasmas were employed to clean the diamond surfaces.

The single crystal diamond wafers, 3x3x0.5 mm, type IIB, with (111) orientation, were polished in 0.25 mm diamond grid and chemically cleaned prior to loading into the vacuum. The chemical cleaning procedure consisted of a 10 min. etch in fuming sulfuric acid, to remove wax used to hold the diamond in the polishing process, a 45 min. etch in fuming chromic acid, to remove graphitic material and concluded by a 10 min. etch in aqua regia to remove metal contaminants. The chromic acid was produced by saturating sulfuric acid with CrO_3. Once in vacuum the sample was further cleaned in a H and Ar plasma before Ti was deposited. The diamond thin films used in this study were grown in a hot filament system. These samples were loaded into the vacuum without *ex situ* cleaning. The samples were however annealed *in situ* to above 750°C for 10 min. and exposed to an H/Ar plasma for 30 min. prior to Ti deposition. All the samples were mounted with Ta wire on a Molybdenum sample holder. Spectra were obtained for increasing titanium coverages until the diamond features in the spectrum were totally replaced by Ti features. For the annealing study a 30Å layer of Ti was deposited and consequently annealed at increasing temperatures in 100°C increments, for 5 min., after which spectra were obtained.

C. Results and Discussion

In order to determine the Schottky barrier height from ARUPS data, it is necessary to determine the position of the valence band edge in the spectra. The uv-photoemission spectrum of single crystal diamond C(111) at surface normal emission is shown in Fig. 1. The valence band edge can be clearly distinguished by the onset of emission at about 1 eV below the Fermi level. The valence band edge position was determined by linear extrapolation of the slope to zero and was found to be 8.1 eV above the strong peak near 8.5 eV. The valence band position was expressed relative to this peak since it remained visible for increasing titanium coverages. In the same figure a spectrum is shown of the C(111) surface at an angle of 30° off

normal along the [110] direction. In this spectrum, the onset of emission shifted -0.6 eV while the strong peak shifted +0.3 eV, the difference between the onset of emission and the reference peak is found to be 7.2 eV. We suggest that the differences in the onset are caused by a downward dispersion of the valence band edge away from the G point in the bandstructure [7]. The spectrum at surface normal emission reflects the valence band at the G point and shows therefore the valence band maximum. A spectrum of a diamond thin film is shown in Fig. 1. For the film, the onset of the emission appears at 7.5 eV above the main peak. We suggest that this is due to the fact that the diamond thin film consists of randomly oriented crystals, which makes the spectrum of diamond thin films in effect equivalent to an angle integrated spectrum of single crystalline diamond. The relative energy of the valence band to the strongest feature of the ARUPS for single crystal diamond at normal emission angle was therefore used to determine the valence band maximum. The determination of the valence band maximum and hence the Schottky barrier height is less accurate however, since the position of the main peak is also angle dependent, as noted above.

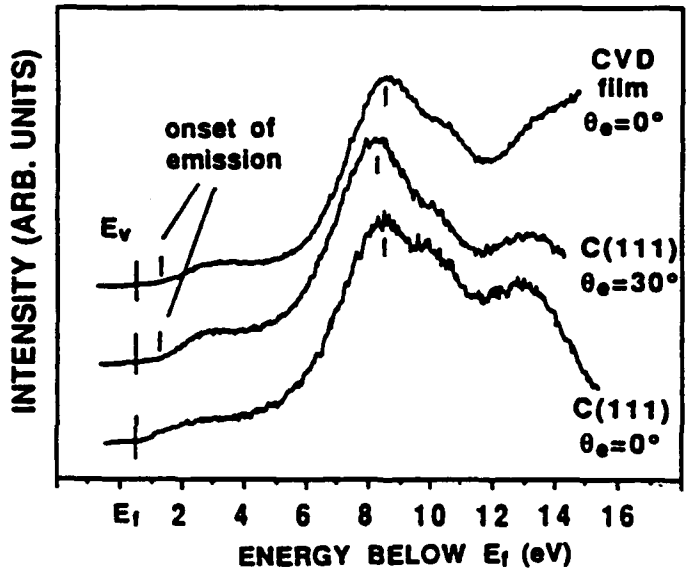

Figure 1. ARUPS spectra of C(111) at normal emission and at 30° off normal, along the 110 direction and of diamond thin film. The solid line shows the position of the valence band maximum, derived from the onset of the C(111) spectrum at surface normal. The vertical lines show the onset of the of the other spectra.

In order to determine the Schottky barrier height, titanium was deposited at room temperature on the single crystal diamond (Fig. 2) and the diamond thin film (Fig. 3). After the first deposition of titanium on the C(111) surface no titanium features could be discerned although the spectrum shifted by 0.45 eV toward lower energies. After further deposition a sharp Fermi edge developed, due to emission from the d-band of titanium. The diamond

valence band energy was determined using the method described above, and a barrier height of 1.0±0.2 eV was deduced. Following the first deposition of <1Å of titanium on the diamond thin film, no titanium could be detected in the ARUPS spectrum, and the spectrum was found to shift 0.35 eV toward lower energies. After further titanium deposition the Fermi level developed while the diamond features were attenuated but still visible. Again, from these spectra, the diamond valence band maximum was determined, and a Schottky barrier height of 0.9 (+0.5/-0.2) eV was found for titanium on the diamond thin film. The asymmetry in the error is related to the fact that the main peak position is angle dependent.

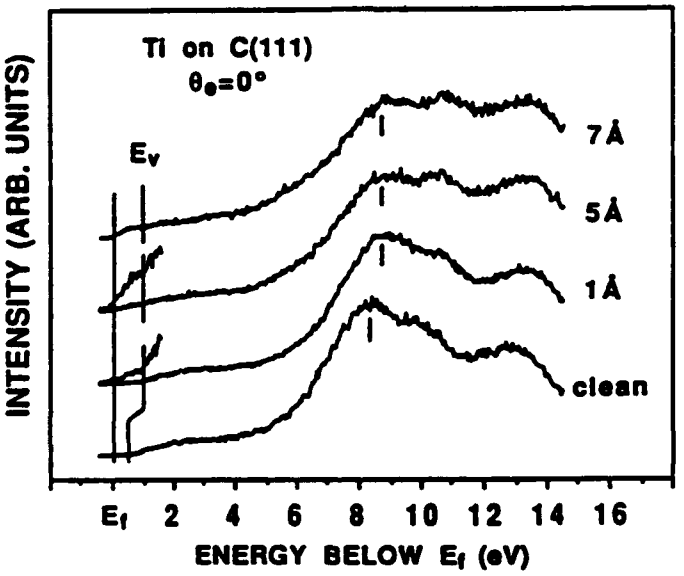

Figure 2. Normal emission spectra of C(111) as a function of titanium coverage.

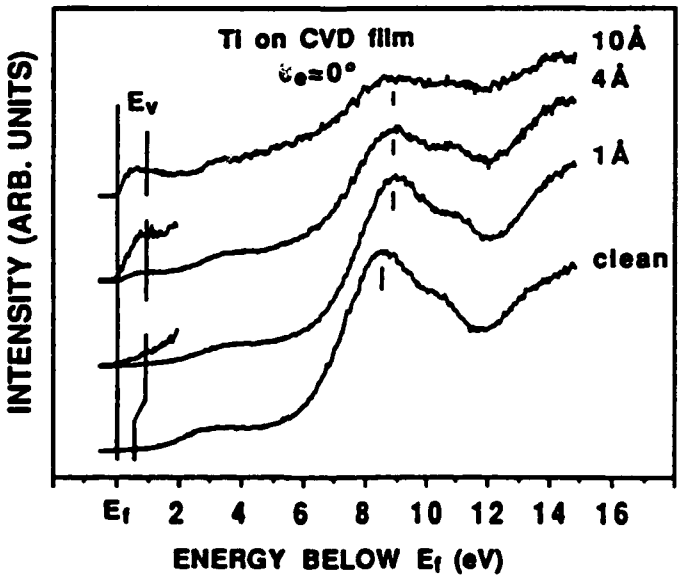

Figure 3. Normal emission spectra of diamond thin film as a function of titanium coverage.

ARUPS spectra of the annealing of a 30Å layer of titanium on a diamond thin film are shown in Fig. 4. The emission at the Fermi edge is again due to the titanium d-band. It has been suggested that the broad peak near -5.5 eV is due to a contamination of the deposited titanium layer, possibly oxygen or hydrogen [8]. No diamond features could be discerned. Subsequent spectra were obtained after annealing the film at increasing temperatures, at 100°C increments. After annealing the film to 400°C a peak starts to appear around -3.5eV and gets more pronounced after annealing to higher temperatures for 5 minutes at a time. This peak is associated with Ti-C bonding [9] and shows the development of Ti-carbide formation which reaches its completion after a 600°C anneal. This correlates well with the transition from rectifying behavior to ohmic behavior as described by Gildenblat [5].

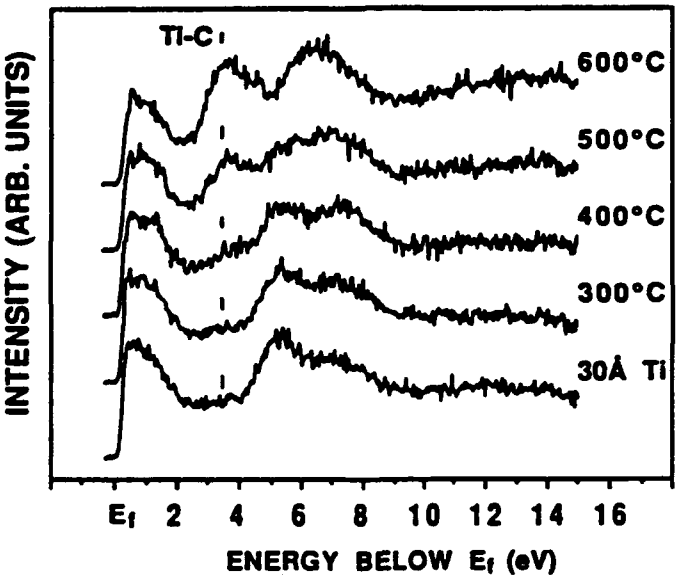

Figure 4. Normal emission spectra of diamond thin film with 30Å Ti as a function of annealing temperature. The peak appearing at 3.5 eV below the Fermi level is indicative of Ti-C formation.

The electron affinity of the surface is also manifested in the ARUPS spectra. In figure 5 we observe that on the low energy end of the spectrum, around -16 eV, a sharp peak develops after the first titanium doses. Then for increasing titanium coverages the peak is attenuated. We attribute this peak to a titanium-induced negative electron affinity. Before the titanium deposition the Fermi level at the surface is 0.5 eV above the valence band edge. The vacuum level was determined from the low energy cutoff point of the emission, and is found to be about 5.5 eV above the valence band edge. Using a value of 5.45 eV for the bandgap of diamond, we find, therefore, the vacuum level to be slightly above the conduction band edge,

and electrons that are quasi-thermalized to the bottom of the conduction band are unable to escape the surface. After the first sub-monolayer of titanium is deposited the Fermi level is pinned at 1.0 eV above the valence band edge and the work function is now determined by the work function of the titanium. Using the value of 4.33 eV for the work function of bulk titanium we find that the vacuum level of the surface now lies 0.2 eV below the conduction band edge and quasi-thermalized electrons can escape, causing the sharp peak in the spectrum. For increasing coverages more electrons thermalize down into the lower energy levels that are available in the titanium. Consequently the intensity of the peak reduces as the titanium thickness increases.

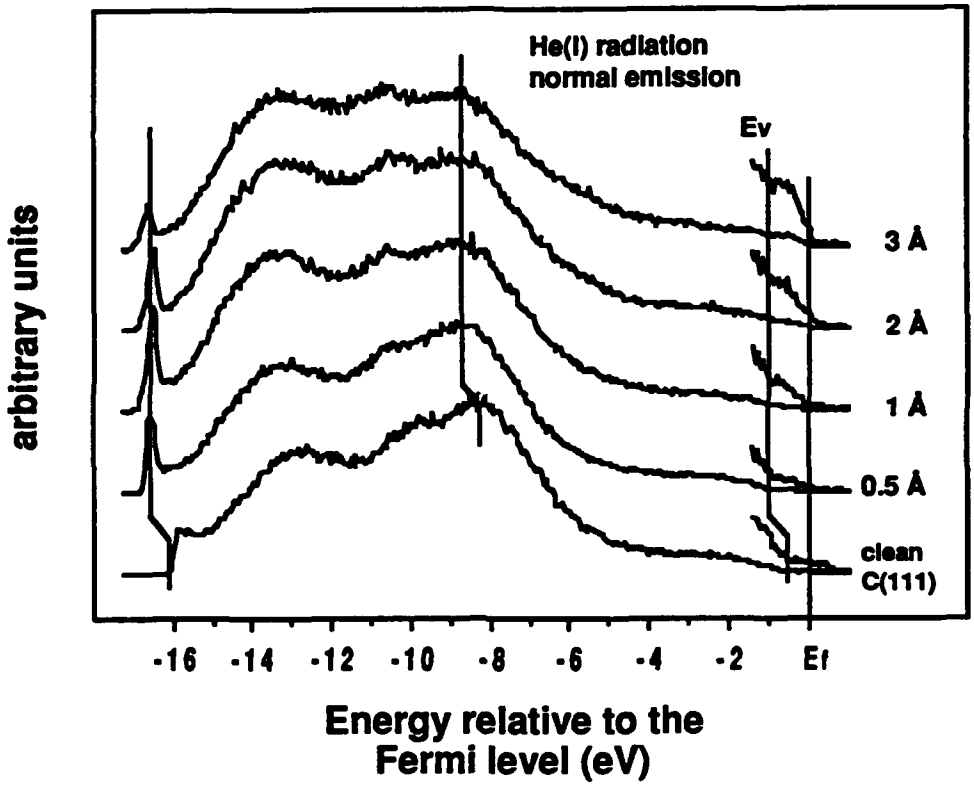

Figure 5. Surface normal emission ARUPS spectra of titanium on diamond (111) for increasing titanium thicknesses

D. Conclusions

Using ARUPS the Schottky barrier height was determined for titanium on both single crystal diamond and diamond thin film. The Schottky barrier height of titanium on single crystal diamond was found to be 1.0±0.2 eV which compared well with the value of 0.9 (+0.5/-0.2) eV found for titanium on diamond thin film. Also the transition from titanium to titanium-carbide was observed to occur for a 30Å layer of Ti on diamond thin film after a 600°C anneal. The onset of the interface reactions were observed at 400°C. This study shows

that it is possible to obtain a negative electron affinity on diamond (111) by depositing a transition metal. For this to occur, it is necessary that the Schottky barrier height plus the workfunction of the metal be less then the bandgap of diamond, and this is apparently the case for Ti on diamond (111).

E. Future Research Plans/Goals

For currently proposed device structures in diamond it is necessary to obtain both Schottky and ohmic contacts to p-type diamond. While reliable n-type doping has not been obtained it will also be important to obtain ohmic contacts to n-type diamond (or electron injecting contacts to high resistivity diamond). This will be particularly important for devices which utilize the negative electron affinity surfaces to achieve cold cathode emission. Since a major potential application of diamond electronic devices is high temperature or high power applications, it is necessary that the contacts are stable at high temperature.

For obtaining stable Schottky or ohmic contacts to p-type diamond, we propose to study the microstructural and electrical properties of various metals (Ti, Ni, Pt), metal silicide ($TiSi_2$ and $NiSi_2$) and semiconductor (Si, SiGe alloys) contacts to homoepitaxial CVD diamond thin films. The direct metal films should form Schottky barriers. Interface reactions may lead to either ohmic or "leaky" Schottky behavior. The silicide compounds offer the possibility of a more chemically stable interface which could result in optimal high temperature operation. The semiconductors offer the option of using well established contacts. Ti and Pt and their silicides were chosen for this study because these metals are often used in semiconductor technology. We have previously established that Ni can be grown epitaxially on diamond and $NiSi_2$ exhibits a cubic lattice structure. The contact materials will be deposited by MBE techniques. The development of the interface will be measured in situ with surface analytical probes in UHV environments. The electronic states at the interface will be established by angle-resolved ultraviolet photoemission spectroscopy (ARUPS) and STM-Ballistic Electron Emission Microscopy (BEEM) techniques. The chemical properties will be determined by AES, LEED and XPS. The structural properties will also be measured with Raman spectroscopy. The morphological aspects will be measured with STM and TEM. The macroscopic barrier heights will be determined by I-V and internal photoemission (or photoresponse) measurements. The correlation of the interface atomic structure and chemistry with the observed electrical properties will be established.

An important aspect of this study is the complete characterization of the initial diamond surface. We note that the cleaning and characterization in the task related to surface electronic states and electron affinity address this issue. The films that will be deposited will be studied from submonolayer coverages up to thicknesses of ~400Å.

Since most metals or metal compounds have electron workfunctions of ~4eV, a different approach is necessary for obtaining ohmic contacts to n-type diamond or for electron injecting contacts to high resistivity (undoped) diamond. The method currently employed involves producing a high resistance region by implanting C into the surface. A high field will then be largely doped over this region and electron injection into the conduction band can occur. Several alternative approaches to be considered in this study include (1) using a low workfunction metal, (2) using very thin wide bandgap oxides or nitrides between the metal and diamond, (3) Using an n-type wide bandgap semiconductor as an intermediate layer.

F. References

1. Y. Mori, H. Kawarada, A. Hiraki, Appl. Phys. Lett **58**, 940 (1991)
2. T.P. Humphreys, H. Jeon, R.J. Nemanich, J.B. Posthill, R.A. Rudder, D.P. Malta, G.C. Hudson, R.J. Markunas, J.D. Hunn and N.R. Parikh, Mat. Res. Soc. Symp. Proc. **202**, 463-468 (1991).
3. T.P. Humphreys, J.V. LaBrasca and R.J. Nemanich, K. Das and J.B. Posthill, Jpn. J. Appl. Phys. (1991).
4. K.L. Moazed, R. Nguyen, J.R. Zeidler, IEEE Electr. Dev. Lett. **9**, 350 (1988)
5. G. Sh. Gildenblat, S. A. Grot, C. W. Hatfield, A.R. Badzian, T. Badzian, IEEE Electr. Dev. Lett. **11**, 371 (1990)
6. H. Shiomi, H. Nakahata, T. Imai, Y. Nishibayashi, N. Fujimori, Jpn. J. Appl. Phys., Part 1 (Regular Papers & Short Notes) **28**, 758 (1989)
7. G.S. Painter, D.E. Ellis, A.R. Lubinsky, Phys. Rev. B **4**, 3610 (1971)
8. D.E. Eastman, Solid State Comm. **10**, 933 (1972)

VII. Modeling and Characterization of Electronic Devices Fabricated from Semiconducting Diamond Thin Films

A. Introduction

The RF performance potential of electronic devices fabricated from semiconducting diamond thin films has been under investigation. So far, the microwave and millimeter wave performance of diamond MESFETs and IMPATT diodes have been investigated in detail. This work has made use of existing theoretical device models for these devices, but the existing device models have required extensive modification with appropriate algorithms to permit the models to be used for this purpose. The models are ideal for this investigation since they are based upon device physics. Therefore, the models permit the dc and RF performance of the devices to be investigated as a function of device structure, doping details, and operating parameters. Along with the RF performance predictions, factors that limit device operation have been of interest.

The most significant limitation that currently exists is the availability of suitable device quality thin films. Although diamond material growth technology is rapidly evolving, it is still not sufficiently advanced to produce the necessary epitaxial layers for device fabrication.The optimum RF performance is predicted to be attainable from n-channel MESFET devices and pn junction IMPATT diodes. The use of semiconducting n-type material, in particular, is attractive due to superior electron transport characteristics compared to that of mobile holes. Despite many reports in the literature, however, there is significant controversy over whether suitable n-type dopants can be found. Most reports of semiconducting n-type diamond are now generally believed to be the result of crystal damage or crystal imperfections, such as dislocations, etc., rather than the effects of activated donor impurities. The difficulty in producing suitable n-type semiconducting crystals has resulted in interest in fabricating devices from p-type material. Natural diamond is often p-type due to boron impurities and synthetic diamond can be doped with boron with relative ease. It is likely, therefore, that the first high performance electronic devices fabricated in diamond will be MESFET or MOSFET devices with p-type conducting channels. Most of the device results presented in the literature, to date, have been such

transistor structures on p-type diamond, and much current work in progress is directed towards the development of p channel field-effect devices on both natural and synthetic p-type material, due to the relative ease of obtaining suitable crystals.

The use of p-type material presents an interesting problem. Most investigations of boron impurities in diamond (e.g., doping by ion-implantation) indicate an activation energy of about 0.37 eV. This, in turn, indicates that the device must be operated at high temperatures (about 500 °C) in order to activate the impurities. Operation at elevated temperature, however, results in rapid degradation of the hole mobility, which decreases with temperature according to a $T^{-2.8}$ law. This, in turn, will reduce the channel current that can flow in the device, thereby significantly reducing the RF output power attainable. This issue has been addressed by investigation of device operation at elevated temperature.

Another limitation associated with the operation of field-effect transistors relates to the breakdown characteristics of the device. Generally, device breakdown is assumed to be due to semiconductor material breakdown. This is certainly true for well designed diodes. However, for field-effect transistors it is possible to have device breakdown occur that is dominated by surface effects. This can occur essentially in parallel with material breakdown. If the surface phenomenon occurs at a lower potential, the surface breakdown mechanism will dominate and can prevent the material from developing it's full potential. We believe that this, in fact, occurs and limits the performance so far reported for diamond field-effect transistors.

The thermal limitation has been investigated and previously reported for MESFETs operating up to 500 °C. The calculations have been extended to 650 °C and are reported here. However, most research over the past few months has concentrated upon developing an explanation for the breakdown phenomena in MESFETs. This work is directed towards developing a model for this phenomena that could possibly lead to a device design that would permit the necessarily large bias voltages to be applied to the device.

B. Investigation Procedure

Physics based device simulators are used to investigate the microwave and mm-wave performance of the devices. A large-signal model based upon numerical solution techniques has been developed and applied to investigate the performance of the IMPATT diodes. The results of this study have been previously reported. In summary, it was determined that up to about 100 GHz diamond IMPATT diodes are capable of about 5-10 times the RF power available from similar devices fabricated from Si, GaAs or InP. Above 100 GHz performance degrades due to the spreading of the avalanche region and the RF output power from diamond and Si IMPATTs are similar. The dc to RF conversion efficiency of diamond IMPATTs is similar to that obtained from Si diodes. RF performance was investigated up to 220 GHz.

For investigation of the RF performance of diamond MESFETs a large-signal device/circuit simulator was used. The simulator is based upon solutions to the semiconductor device equations and is, therefore, based upon physical device operation. The simulator has previously been used to predict the microwave performance of GaAs microwave MESFETs and has produced results in excellent agreement with experimental data. For this work the simulator was modified to allow for the investigation of diamond devices.

The model accepts data describing the geometry and doping profile of the diode and with the appropriate material data, produces information about the operating characteristics of the device. Both ac and dc solutions are obtained from the model. The MESFET is embedded in a realistic dc and RF circuit so that impedance tuning considerations are included. The principal output data of the RF simulation are the input and output RF impedances, the RF output power, the power-added efficiency, and the gain. In this work the operation frequency was set to 10 GHz.

The investigation of the performance limitations of diamond MESFETs requires modifications to the model code. To investigate the thermal operation of the device a thermal resistance model, and extensive modifications to the model code in order to include the thermal resistance model, were required. This was performed and previously reported. The limitations due to breakdown also requires a new model for this phenomenon. This work is underway and recent advances are reported in the Discussion Section.

C. Results

The X-band power MESFET previously reported and designed to produce maximum power-added efficiency under class A operating conditions at 10 GHz was further investigated. In particular, the operation of the device at 650 °C was investigated. This temperature was selected as being representative of the conditions to achieve high carrier activation. The device has a gate length of Lg = 0.5 μm and a gate width of W = 1 mm. These dimensions are typical of those used for GaAs power MESFETs. The material parameters for operation at a temperature of 650 °C were determined and used to predict device operation at this temperature. Full activation was not assumed and the boron doping level would need to be sufficient to result in a channel hole density of $4x10^{17}$ cm^{-3}. The actual boron density could, therefore, could be greater than the hole density, although at this temperature high activation is expected.

The RF operation of the device was simulated by embedding the device in an RF circuit and tuning the output impedance for maximum power-added efficiency at the one db compressed RF output power point. The RF performance of the device is then determined by holding the circuit impedances fixed, while the input RF power is varied until the device is driven into saturation. The results of the calculations for the 10 GHz, 650 °C operation are shown in Fig. 1. The maximum RF output power at the one db compression point is 31.0 dbm or 1.3 W/mm. This is significantly reduced compared to operation predicted for lower operating temperature, but is still comparable to the RF power obtained with GaAs

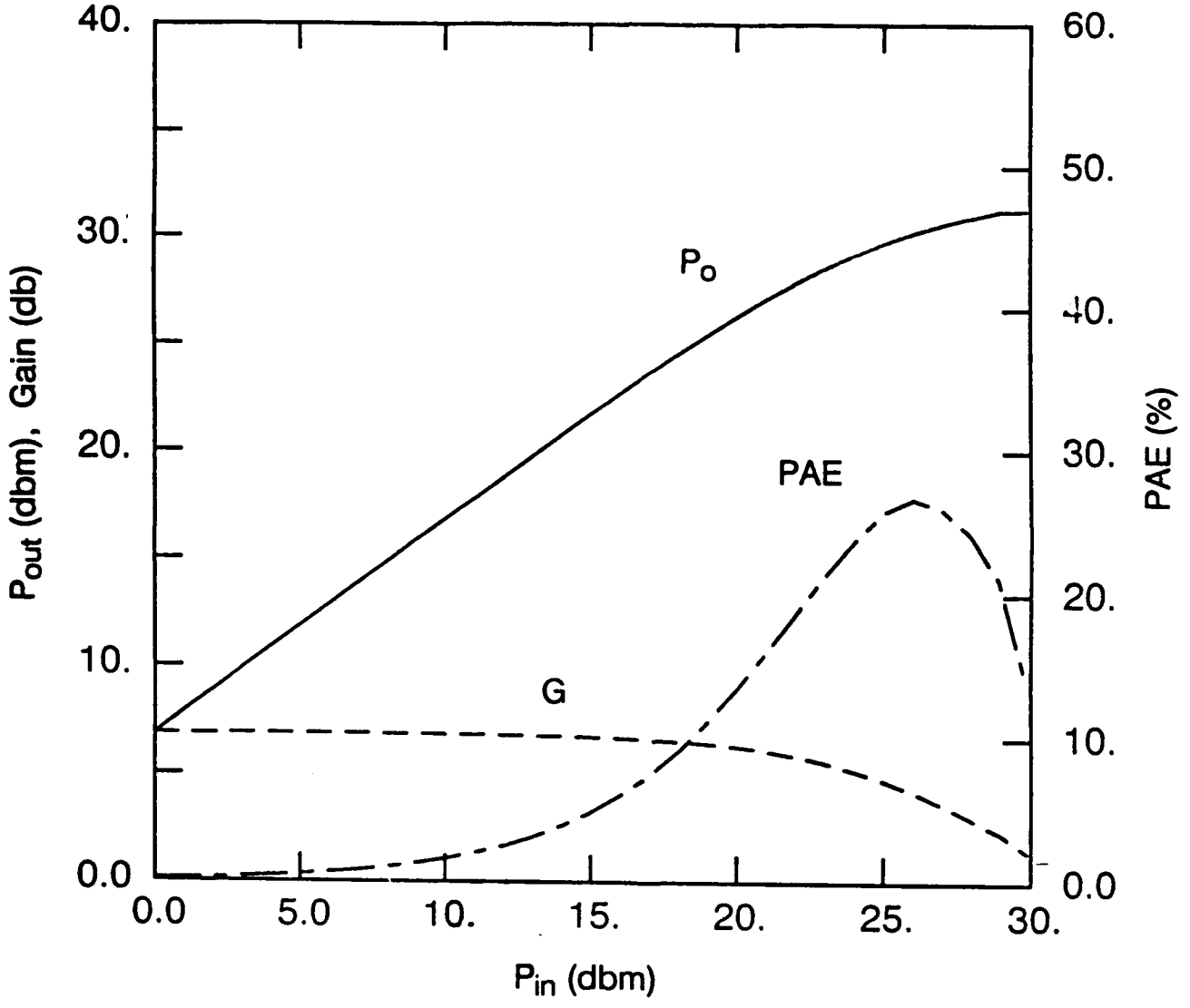

Figure 1. RF operation of a P-type diamond MESFET at 650°C (Lg=0.5 μm, W=1 mm, Frequency=10 GHz, Class A operation).

MESFETs, which so far have demonstrated about 1.7 W/mm. It should be noted, however, that the operation predicted for lower operating temperature may not be possible due to the carrier activation issue. The linear gain is shown in Fig. 1 is about 7 db and the maximum power-added efficiency is about 27%. This performance is quite respectable, considering the high operating temperature. A summary of the room temperature, 500 °C and 650 °C operation is presented in the following table.

P-Type Diamond MESFET
Class A Operation at 10 GHz

Room Temperature	500 °C	650 °C
Vds = 40 v	Vds = 30 v	Vds = 25 v
BV_{gd} = 92 v	BV_{gd} = 70 v	BV_{gd} = 60 v
Po = 37.7 dbm	Po = 32.8 dbm	Po = 31.0 dmb
PAE_{max} = 50.6 %	PAE_{max} = 33.2 %	PAE_{max} = 26.8%
G = 12.2 db	G = 8.1 db	G = 6.8 db

D. Discussion

The RF performance predicted for the diamond MESFETs assumes that sufficient bias can be applied to the device to produce charge carrier saturation. Although drain bias voltages need only be in the range of 5-10 v to achieve these conditions, difficulty has been experienced in achieving carrier saturation in the few experimental devices reported to date. A significant gate leakage problem has been found to exist. The leaky gate prevents large drain bias voltages from being applied. This, in turn, prevents current saturation conditions

from being obtained, thereby yielding poor device performance. Attempts to avoid this problem have generally been focused upon the utilization of a MOSFET or MISFET structure, where an insulator is used to isolate the gate metal from the diamond conducting channel. This restricts the gate leakage current and allows larger drain bias voltages to be applied. Limited improvement has been achieved with the use of SiO_2 as the insulator, yielding a diamond MOSFET. The insulators do not, however, completely solve the problem and drain bias voltages sufficient to obtain the RF performance predicted by the simulator can not be applied.

The diamond semiconductor has a large critical electric field for breakdown, as indicated in Fig. 2. This figure shows the avalanche ionization rates for charge carriers in various semiconductors. The rates for diamond were taken from the results of diamond pn junctions operating in avalanche breakdown, as reported in the literature. The ionization rates indicate a critical electric field for breakdown in excess of 10^6 v/cm. Such a breakdown field would produce a gate-drain breakdown voltage in the range of 100 v for the device investigated in this work. This breakdown voltage would allow the bias voltages used in this work to be applied.

We believe that the gate leakage problem results from a breakdown mechanism that occurs in parallel with the normal avalanche breakdown mechanism. The parallel breakdown occurs at a much reduced applied bias condition and limits the drain bias that can be applied. The breakdown issue is illustrated in Fig. 3, which indicates the areas of the device where breakdown can occur. The normal breakdown for a Schottky junction is indicated as region 1. The breakdown voltage for this condition is much larger than observed in practice, even for GaAs MESFETs. Breakdown can occur at the drain electrode, or at the channel/substrate interface. Neither of these mechanisms, however, commonly occur. Breakdown in experimental devices has been localized to the region near the gate electrode at the semiconductor surface, as indicated in Fig. 4. The electric field at the surface can become very large due to the device geometry, and breakdown conditions

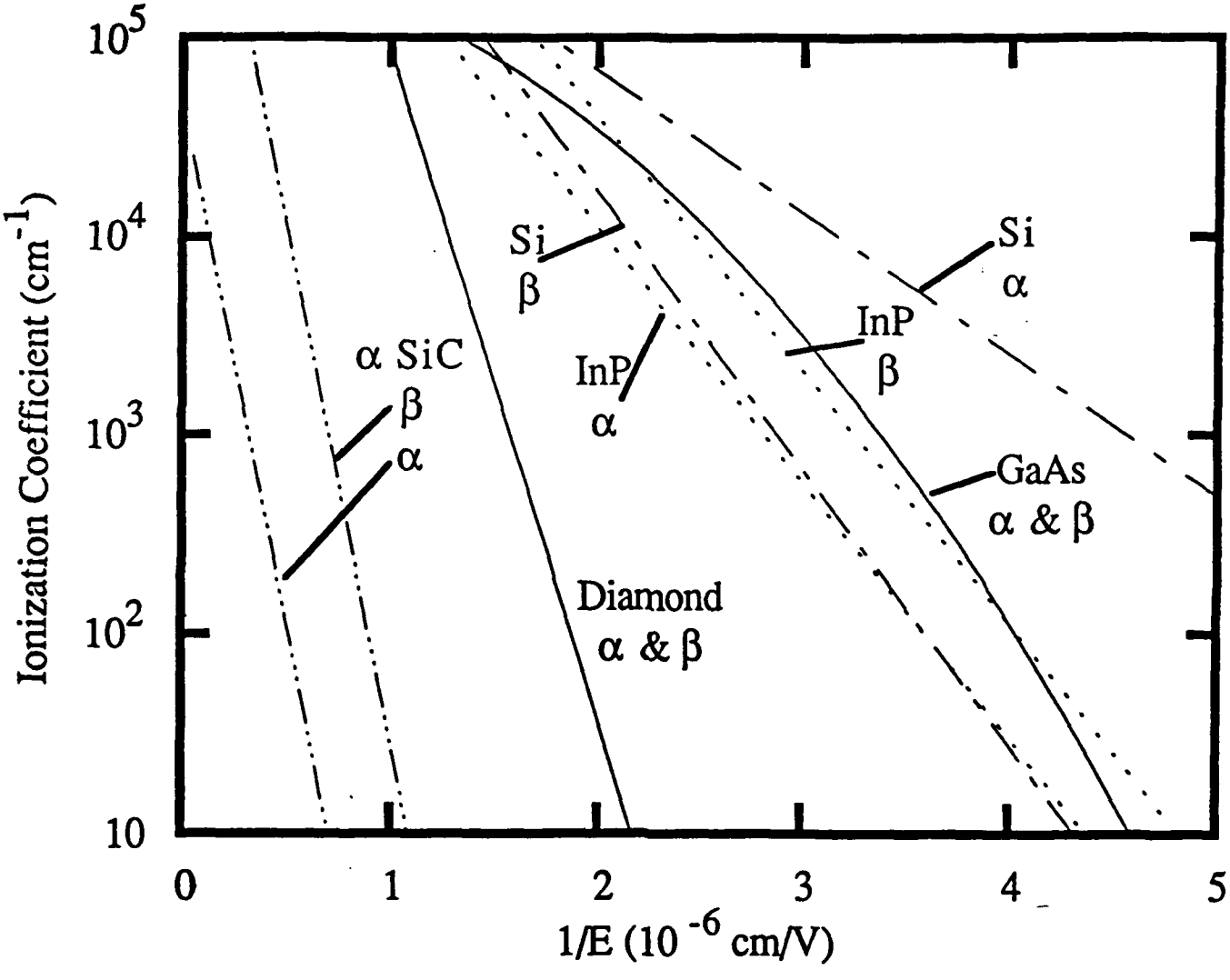

Figure 2. Ionization rates versus electric field for several semiconductors.

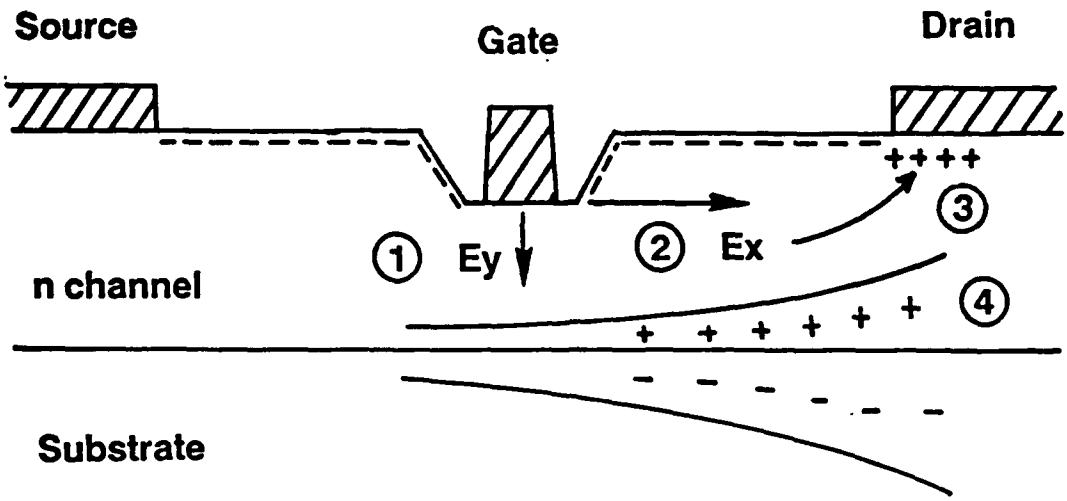

① Bulk Gate Breakdown

② Surface Breakdown

③ Drain Breakdown

④ Channel/Substrate Breakdown

Figure 3. Sketch of a MESFET showing regions of possible breakdown.

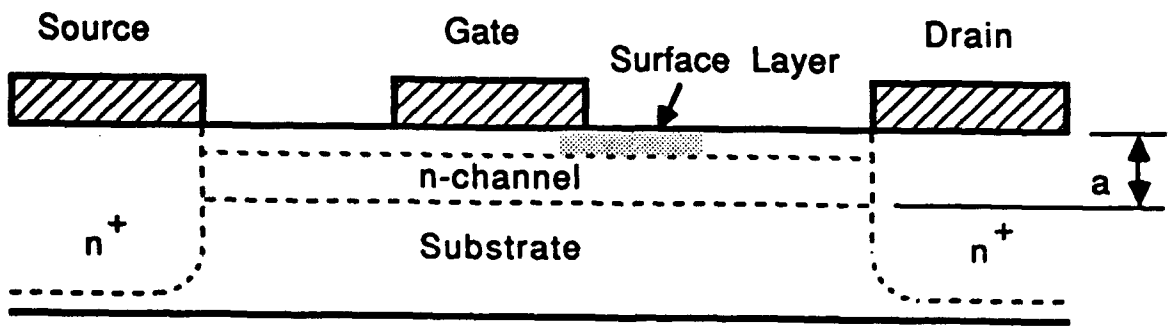

Figure 4. Sketch of a MESFET indicating surface region responsible for gate leakage.

can easily be obtained. This is illustrated in Fig. 5, which shows electric field profiles in the channel of a MESFET as a function of position for various bias conditions. The electric field at the gate edge is observed to be large, and breakdown conditions can easily be achieved.

We are currently working on a model to describe the surface breakdown phenomenon. The new model is based upon a combination of thermal tunneling, as well as avalanche breakdown. We believe that charge carriers tunnel from the gate metal to the surface of the semiconductor. The charge carriers can then flow along the surface of the semiconductor to the drain electrode, thereby creating the gate leakage current. Preliminary results of a simple formulation of the model give results in qualitative agreement with experimental data for GaAs MESFETs. We believe that this model will describe the breakdown behavior of diamond MESFETs.

According to this model, if the gate leakage current is to be reduced, it will be necessary to design a surface passivation that will reduce the electric field at the gate edge. Also, a passivation that prevents surface conduction is necessary. Most dielectric passivations, however, allow conduction at the dielectric/semiconductor interface. This issue is currently under investigation and will be discussed in more detail in future reports.

E. Conclusions

The RF operation of a p-type diamond MESFET operating under class A circuit tuning conditions at 10 GHz was further investigated. Due to the relatively high activation energy of boron in diamond high operation temperatures may be required in order to obtain sufficient charge carriers to allow the device to function with good performance. For this reason the operation of the device was simulated at elevated temperature up to 650 °C. It was found that although elevated temperature results in significant RF performance degradation, the RF performance at 650 °C is still adequate for practical applications. The

Electric Field Distribution in a GaAs MESFET

At the Surface (Y=0 micron), In the Channel (Y=0.18 micron)

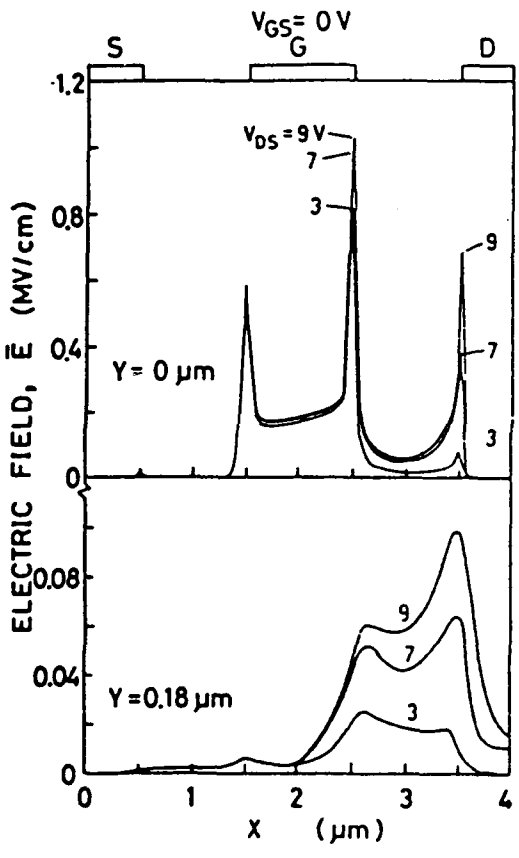

Vgs=0 v, Vds=3,7, and 9 v

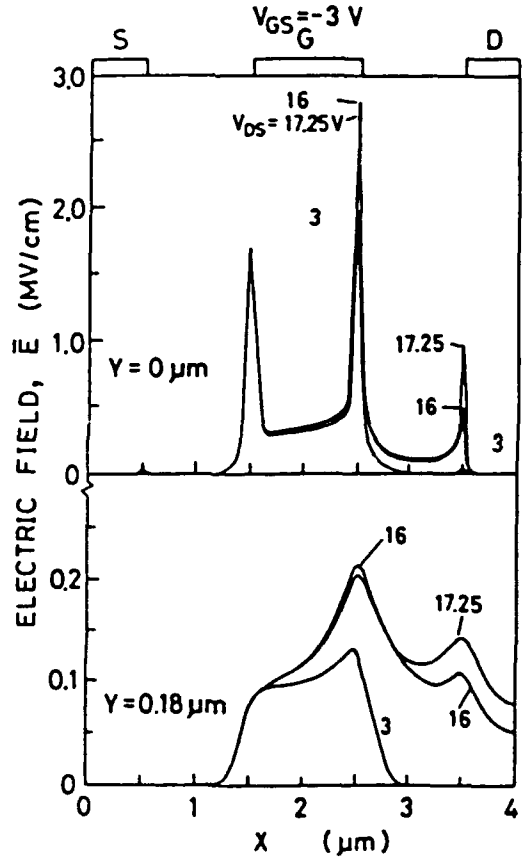

Vgs=-3.0 v, Vds=3,16, and 17.25 v

Figure 5. Electric field distribution in a GaAs MESFET. The surface electric field is indicated by the Y=0 contours.

results of this investigation indicate that p-type diamond MESFETs offer considerable potential for use in microwave, high temperature applications.

The realization of the RF performance predicted by the simulator is dependent upon the ability to apply sufficient bias to achieve current saturation. Also, bias voltages above this value are necessary to achieve large RF output power, which increases directly in proportion to the drain bias. Experimental devices reported so far, however, demonstrate a leaky gate phenomenon. The leakage problem is under investigation and a model to describe the behavior is being formulated. We believe that the leakage problem is due to charge carrier tunneling from the gate metal to the surface of the diamond and surface conduction to the drain electrode. Techniques for reducing the leakage are under investigation.

F. Future Research Plans and Goals

The dopant activation issue will be investigated in more detail by means of simulations of the density of free charge carriers as a function of temperature. This issue must be addressed, along with the question of gate-drain breakdown voltage in order to obtain a realistic picture of the potential of these devices for microwave and mm-wave applications. The development of the gate-drain breakdown and surface conduction model will be continued. Also, techniques for reducing the surface conduction by application of suitable passivation layers will be investigated. We expect to propose leakage conduction reduction techniques in the near future.

Appendix A. List of Abstracts

The following articles may be obtained from the authors.

MICROSTRUCTURES AND DOMAIN SIZE EFFECTS IN DIAMOND FILMS CHARACTERIZED BY RAMAN SPECTROSCOPY

R. J. Nemanich, L. Bergman, Y. M. LeGrice, K. F. Turner and T. P. Humphreys
(Submitted to SPIE, 1991)

The issues related to Raman scattering characterization of the microstructure of diamond thin films are reviewed. The optical effects of the transparent/absorbing composite of sp^2/sp^3 bonded material is discussed. Then the dependence of the Raman spectra on the microcrystalline size is described. The comparison is made with crystalline Si, and the analysis is applied to series of diamond films. Lastly micro-Raman scattering from the initial stages of diamond film growth are described, and the results are correlated with STM measurements of the nuclei. Surface enhanced Raman scattering is applied to examine the regions between diamond nuclei.

HIGH TEMPERATURE RECTIFYING CONTACTS USING HETEROEPITAXIAL Ni FILMS ON SEMICONDUCTING DIAMOND

T.P. Humphreys, J.V. LaBrasca, R.J. Nemanich, K. Das and J.B. Posthill
(Reprinted from Japanese Journal of Applied Physics, 30 No. 8A, August, 1991, pp. L.1409-L.1411)

The first results pertaining to the fabrication of high-temperature rectifying contacts using heteroepitaxial Ni films deposited on natural p-type *semiconducting* diamond substrates are reported. The contact diodes were deposited at 500°C by the thermal evaporation of Ni from a W filament in ultra-high vacuum. The epitaxial nature of the deposited Ni layers has been established from an inspection of *in situ* low-energy electron diffraction (LEED) patterns. The Ni films exhibit excellent adhesion properties with the underlying diamond substrate. As evidenced by current-voltage (I-V) measurements stable rectifying characteristics for the Ni/diamond contacts were observed in the 25-400°C temperature range.

SURFACE TOPOGRAPHY AND NUCLEATION OF CHEMICAL VAPOR DEPOSITION DIAMOND FILMS ON SILICON BY SCANNING TUNNELING MICROSCOPY

K.F. Turner, Y.M. LeGrice, B.R. Stoner, J.T. Glass, and R.J. Nemanich
(J. Vac. Sci. Technol. B9 (2), Mar/Apr 1991)

The surface topography of diamond thin films deposited on silicon have been charted by scanning tunneling microscopy (STM). This study addresses the initial nucleation of diamond growth on Si, and the faceted structure of the diamond films. The results were obtained from an in-air STM system with tunneling currents between 0.2 and 3 nA. For studies of the diamond nucleation, samples were prepared by timed growth up to 60 min in a microwave plasma chemical vapor deposition (CVD) system. Diamond films with thicknesses in the 1-2 μm range were prepared by hot-filament CVD and examined by STM to determine the morphology of the diamond growth surface. The presence of diamond was verified by Raman spectroscopy. The STM images show that the surface is uniformly affected in the first 30 min of growth and diamond nuclei are identified after 60 min of growth. The thick films showed topography with facets on the surface similar to those seen from scanning electron microscopy results. The surface of these facets have been examined as well as the area between the facets. Elongated ridge structures are observed between different facets on the surface.

SELECTED-AREA HOMOEPITAXIAL GROWTH AND OVERGROWTH ON Si PATTERNED DIAMOND SUBSTRATES

R.A. Rudder, J.B. Posthill, G.C. Hudson, D. Malta, R.E. Thomas and R.J. Markunas, T. P. Humphreys and R. J. Nemanich

(Proceedings of the Second International Conference on New Diamond Science & Technology, edited by R. Messier and J.T. Glass, Materials Research Society Int'l. Conference Proceedings Series (MRS, Pittsburgh, PA, 1991)

Epitaxial diamond overgrowth on Si patterns on natural diamond substrates has been demonstrated using low pressure rf plasma-assisted chemical vapor deposition. The plasma-assisted technique uses a 13.56 MH_Z rf generator and inductive coupling to excite gas mixtures of H_2, CH_4 and CO at a reduced pressure of 5 Torr. The overgrowth was approximately isotropic, extending over the Si pattern by 0.45 μm and above the Si layer by 0.50 μm.

OBSERVATION OF SURFACE MODIFICATION AND NUCLEATION DURING DEPOSITION OF DIAMOND ON SILICON BY SCANNING TUNNELING MICROSCOPY

K.F. Turner, B.R. Stoner, L. Bergman. J.T. Glass, and R.J. Nemanich

(J. Appl. Phys. 69 (9), May 1991)

The surface topography of silicon substrates after the initial stages of diamond growth, by microwave plasma enhanced chemical vapor deposition, has been observed by scanning tunneling microscopy. The initial surfaces were polished with diamond paste before deposition to enhance nucleation, and the scratches were examined. After one half hour growth, the surface showed additional topography over all regions, and widely spaced faceted structures were detected which were attributed to diamond nuclei. The surface between nuclei showed increased roughness with increased deposition time. The faceted nuclei were found along the scratches. The nuclei showed facets which were smooth to within 5 Å. Fingerlike ridge structures were found extending from and in-between some of the nuclei. These structures indicate a mechanism of the lateral diamond growth. The electronic properties of the surface were probed by local *I-V* measurements, and characteristics attributable to SiC were observed.

INTERFACE REACTIONS OF TITANIUM ON SINGLE CRYSTAL AND THIN FILM DIAMOND ANALYZED BY UV PHOTOEMISSION SPECTROSCOPY

J. VanderWeide and R.J. Nemanich

(Applications of Diamond Films and Related Materials, Y. Tzeng, M. Yoshikawa, M. Murakawa, A. Feldman (Editors), Elsevier Science Publishers B.V., 1991)

The reactions of titanium on natural crystals and CVD polycrystalline thin films were studied by uv-photoemission spectroscopy. The focus of this study was to characterize the interface reactions and to determine the Schottky barrier of titanium on diamond, deposited and annealed in UHV. Spectroscopic features attributed to the electronic states of Ti-C were identified, and the formation of titanium carbide was observed as a function of annealing temperature. The onset of a titanium-carbon reaction was observed after the 400°C anneal. A well defined TiC spectra was observed after annealing to 600°C. The Schottky barrier height from Ti on natural p-type diamond (111) was obtained by determining the valence band maximum and the Fermi level, and a barrier height of 1.0±0.2 eV was found.

TITANIUM SILICIDE CONTACTS ON SEMICONDUCTING DIAMOND SUBSTRATES

R. J. Nemanich

(Reprinted from Electronic Letters 15 August 1991, Vol. 727 No. 17 pp. 1515-1516)

Titanium silicide contacts have been deposited on semiconducting (p-type) natural diamond substrates by the code position of silicon and titanium by electron-beam evaporation. Current-voltage (I-V) measurements conducted at room temperature have demonstrated rectifying characteristics. Consistent with the observed small turn-on voltage, the corresponding I-V measurements recorded at 400°C exhibit ohmic-like behavior. However, on subsequent annealing of the titanium silicide contacts at 1100°C in a vacuum of ~10^{-6} Torr for 30 min, stable rectifying I-V characteristics were observed in the 25-400°C temperature range.

OBSERVATION OF LATERAL GROWTH BETWEEN DIAMOND DOMAINS BY SCANNING TUNNELING MICROSCOPY

K.F. Turner, B.R. Stoner, L. Bergman, J.T. Glass, R.J. Nemanich

(To appear in the Second International Conference on the New Diamond Science and Technology, September, 1990)

The surface of diamond thin films deposited on silicon have been examined by scanning tunneling microscopy (STM). This study addresses the growth structures that have been observed between different domains of the films. The results were obtained from an in-air STM system with tunneling currents between 1-2 nA. For studies of the growth morphology of diamond films, films with thicknesses in the 1μm to 2μm range were prepared by hot wire filament CVD. Films grown by a microwave plasma CVD system for growth periods up to 60 minutes were used to study the morphology of the surface during the early stages of growth. The presence of diamond was verified by Raman spectroscopy. The STM images show that the surface is uniformly affected in the first 30 minutes of growth and diamond nuclei are identified after 60 minutes of growth. Similar growth structures were observed in both the initial nucleation samples and the doped samples, and it is postulated that these structures are indicative of the growth mechanisms involved at their respective stages of growth.

RAMAN CHARACTERIZATION OF DIAMOND FILM GROWTH

R.J. Nemanich, L. Bergman, Y.M. LeGrice, R.E. Shroder

(To appear in the Second International Conference on the New Diamond Science and Technology, September, 1990)

The application of Raman spectroscopy for characterizing carbon bonding in diamond thin films is described. The spectral signatures of different carbon bonding structures are described, and the limitations for quantitative characterization of sp^2 to sp^3 bonding is presented. As diamond growth methods improve other aspects of the films require characterization, and it is shown that Raman scattering can be applied for measurement of strain and crystalline domain size. Major issues with regards to film growth include nucleation and the structures of the growth surface. Micro-Raman and micro-photoluminescence measurements can be applied to examine the film surface and the initial nucleation process. Models are discussed which relate the Raman scattering results to the diamond growth process.

CHARACTERIZATION OF TITANIUM SILICIDE CONTACTS DEPOSITED ON SEMICONDUCTING DIAMOND SUBSTRATES

T. P. Humphreys, Hyeongtag Jeon, J. V. LaBrasca, K. F. Turner, and R. J. Nemanich
(Applications of Diamond Films and Related Materials, Y. Tzeng, M. Yoshikawa, M. Murakawa, A. Feldman, Eds., Elsevier Science Publishers B.V., 1991)

The first results pertaining to the growth and characterization of titanium silicide contacts deposited on natural semiconducting diamond substrates are reported. The titanium silicide films were formed by the co-deposition of silicon and titanium in ultra-high vacuum by electron-beam evaporation in a molecular beam epitaxy (MBE) system. The grown layers have been characterized using Raman spectroscopy, scanning tunneling microscopy (STM) and current-voltage (I-B) techniques. In particular, it has been shown from I-V measurements taken at room temperature that the titanium silicide film forms a low-barrier rectifying contact. Consistent with the observed low-barrier height, the corresponding I-V measurements recorded at 400°C exhibit ohmic-like behavior. However, on subsequent annealing of the titanium silicide contacts at 1100°C, stable rectifying I-V characteristics were observed in the 25– 400°C temperature range.

ACETYLENE PRODUCTION IN A DIAMOND-PRODUCING LOW PRESSURE rf-PLASMA ASSISTED CHEMICAL VAPOR DEPOSITION ENVIRONMENT

R. A. Rudder, G. C. Hudson, J. B. Posthill, R. E. Thomas, and R. J. Markunas, R. J. Nemanich, Y. M. LeGrice, and T. P. Humphreys
(Submitted to Electrochemical Society, 1990)

Many workers are studying the importance of acetylene and methyl radicals in the vapor phase growth of diamond. Techniques such as infrared diode laser absorption spectroscopy and multiphoton ionization have been used to examine the gaseous environment of the diamond deposition. In the work reported here, quadrupole mass spectroscopy has been used to monitor the acetylene production during diamond deposition under a low pressure rf-plasma chemical vapor deposition environment.

THE PERFORMANCE OF P-TYPE DIAMOND MESFETs AT ELEVATED TEMPEATURE

R. J. Trew
(1991 WOCSEMMAD Conference, Ft. Lauderdale, FL, Feb. 1991)

The microwave performance of p-type diamond MESFETs operating under class A operation conditions at 10 GHz is investigated. The use of boron dopants allows p-type semiconducting thin films suitable for the fabrication of MESFETs. Boron, however, has a relatively high activation energy and elevated temperature operation may be necessary in order to obtain suitable free charge densities in the MESFET conducting channel. Elevated temperature operation is expected to result in significantly degraded RF performance since holes in diamond demonstrate a $T^{-2.8}$ temperature dependence. In this study RF operation at room temperature and 500°C was simulated. The study reveals that although elevated temperature operation results in degradation, the RF performance possible is still significantly superior to that available from GaAs MESFETs operating at room temperature. At 10 GHz and 500°C the p-type diamond MESFET is capable of producing RF output power, power-added efficiency and gain of 1.9 W/mm, 33% and 8 db, respectively.

THE POTENTIAL OF DIAMOND AND SiC ELECTRONIC DEVICES FOR MICROWAVE AND MILLIMETER-WAVE POWER APPLICATIONS

R. J. Trew, J. B. Yan, and P. M. Mock
(Proc. IEEE, 79, 598-620, May 1991)

There is significant interest in developing microelectronic devices for blue emission, high temperature, high power, high frequency, and radiation hard applications. This interest has generated significant research effort in wide bandgap semiconductor materials, in particular SiC and semiconducting diamond. Both of these materials are similar in crystal structure with half of the carbon atoms in the diamond structure replaced by Si to produce SiC. However, the latter material exists in a host of polytypes, the causes of which are not completely understood. The deposition of monocrystalline diamond at or below 1 atm. total pressure at T<1000 °C has been achieved on diamond substrates, although deposited film has been polycrystalline on all other substrates. For significant application to electronic devices, the heteroepitaxy of single crystal films of diamond and an understanding of mechanisms of nucleation and growth, methods of impurity introduction and activation and further device development must be achieved. The technology of producing SiC is more advanced and the deposition of thin films and the associated technologies of impurity incorporation, etching, and electrical contacts have culminated in a host of solid state devices. In this paper, the potential of SiC and diamond for producing microwave and millimeter-wave electronic devices is reviewed. Both of these materials have been proposed for fabrication of devices capable of producing RF output power significantly greater than can be achieved with comparable devices fabricated from commonly used semiconductors such as Si and GaAs. Theoretical calculations are presented of the RF performance potential of several candidate high frequency device structures: the MEtal Semiconductor Field-Effect Transistor (MESFET), the IMPact Avalanche Transit-Time (IMPATT) diode, and the Bipolar Junction Transistor (BJT).

DIAMOND AND SiC ELECTRONIC DEVICES FOR SEMICONDUCTING POWER APPLICATIONS

R. J. Trew
(Virginia Mountain Chapter Mtg., IEEE Microwave Theory and Techniques Society, Roanoke, VA, Oct. 1991)

The RF performance of MESFET and IMPATT devices fabricated in semiconducting diamond and SiC have been investigated. The results of these investigations indicate that devices implemented in these materials offer the potential for significantly improved RF performance in microwave and mm-wave power applications. In order to achieve this improved performance, however, it is necessary to operate the devices under velocity saturated conditions, which require high bias voltages and currents. Significant dc power dissipation occurs in the device and high operating temperatures are expected. Elevated temperature, in turn, degrades charge carrier transport characteristics and can produce degraded RF performance. In order to examine this effect in detail, thermal models have been included in the device models used to simulate the RF operation of the various devices under consideration. The thermal model requires a knowledge of the thermal resistance of the device. Once the thermal resistance is known the temperature rise can be determined from a calculation of the dc power dissipated in the device. The operation of the device at elevated temperature is then simulated by degradation of the charge carrier transport characteristics according to known temperature functions. Results of the calculations indicate that both diamond and SiC electronic devices are capable of good RF performance at temperatures at least as high as 650°C.

MATERIAL AND DESIGN PARAMETER EFFECTS IN IMPATT DIODES

P. M. Mock ([R. J. Trew] Ph.D. Thesis, North Carolina State University, 1991)

THE POTENTIAL OF SIC AND DIAMOND FOR MICROWAVE POWER MESFETS

J. B. Yan ([R. J. Trew] Ph.D. Thesis, North Carolina State University, 1991)

Appendix B

Distribution List—Annual Letter Report
Contract Number N00014-86-K-0666

Address	Number of Copies
Mr. Max Yoder Office of Naval Research Electronics Program–Code 1114 800 North Quincy Street Arlington, VA 22217	8
Administrative Contracting Officer Office of Naval Research Resident Representative N66005 The Ohio State Univ. Research Ctr. 1314 Kinnear Road Columbus, OH 43212-1194	1
Director Naval Research Laboratory Attention: Code 2627 Washington, DC 20314	6
Defense Technical Information Center Building 5 Cameron Station Alexandria, VA 22314	12
Robert J. Markunas Research Triangle Institute Post Office Box 12194 Research Triangle Park, NC 27709-2194	1
Michael W. Geis Lincoln Laboratories 244 Wood Street P. O. Box 73 Lexington, MA 02173	1
Professor N. Parikh Department of Physics University of North Carolina-CH Chapel Hill, NC 27514	1
Professor Russell Messier 265 Materials Research Laboratory Pennsylvania State University University Park, PA 16802	1
Dr. James Butler Naval Research Laboratory Code 6174 Washington, DC 20375	1
James Mayer Materials Science and Engineering 210 Bard Hall Cornell University Ithaca, NY 14853	1
Dr. Bradford Pate Department of Physics Washington State University Pullmany, WA 99164-2184	1
Professor Pankove Electrical and Computer Engineering University of Colorado Boulder, CO 80309-0455	1
Office of Naval Research Attention: Code 1131M Arlington, VA 22217	1
Naval Research Laboratory Attention: Code 4683 Washington, DC 20375	1
Naval Research Laboratory Attention: Code 6820 Washington, DC 20375	1
Naval Research Laboratory Attention: Code 6211 Washington, DC 20375	1
Naval Research Laboratory Attention: Code 6684 Washington, DC 20375	1

Naval Research Laboratory
Attention: Code 4684
Washington, DC 20375 — 1

Dr. Jim Zeidler
Naval Ocean Systems Center
Attention: Code 7601
San Diego, CA 92152 — 1

Naval Ocean Systems Center
Attention: Code 911
San Diego, CA 92152 — 1

Naval Ocean Systems Center
Attention: Code 56
San Diego, CA 92152 — 1

Dwight Duston
OSD/SDIO/IST
Pentagon
Washington, DC 20301-7100 — 1

DARPA/D.S.O.
1400 Wilson Boulevard
Arlington, VA 22209 — 1

Professor R. F. Davis
Materials Science and Engineering
Box 7907
North Carolina State University
Raleigh, NC 27695-7907 — 1

Professor K. J. Bachmann
Materials Science and Engineering
Box 7907
North Carolina State University
Raleigh, NC 27695-7907 — 1

Professor R. J. Nemanich
Department of Physics
Box 8202
North Carolina State University
Raleigh, NC 27695-8202 — 1

Professor R. J. Trew
Electrical and Computer Engineering
Box 7911
North Carolina State University
Raleigh, NC 27695-7911 — 1

Dr. Sandor Holly
Rocketdyne Division
Rockwell International, MS FA03
Canoga Park, CA 91304 — 1

Professor G. Walrafen
Chemistry Department
Howard University
5325 Potomac Avenue, NW
Washington, DC 20016 — 1

Professor I. Lindau
Synchrotron Radiation Laboratory
Stanford, CA 94305 — 1

A. J. Purde
Texas Instruments
MS 147
P. O. Box 655936
Dallas, TX 75265 — 1

W. D. Partlow
Westinghouse Research
and Development Center
1310 Beulah Road
Pittsburgh, PA 15235 — 1

R. L. Adams
21002 North 19th Avenue
Suite 5
Phoenix, AZ 85027 — 1

Professor John C. Angus
Chemical Engineering
Case Western Reserve University
Cleveland, OH 44106 — 1

Prof. Thomas R. Anthony
General Electric Corporation
Research and Development Center
Building K-1, Room 1CSO
P. O. Box 8
Schnectady, NY 12301 — 1

Yehuda Arie
SRI Sarnoff Center
Princeton, NJ 08540 — 1

P. J. Boudreaux
Laboratory for Physical Science
4928 College Avenue
College Park, MD 20740 — 1

Professor R. F. Bunshaw
University of California
6532 Buelter Hall
Los Angeles, CA 90024 — 1

Ray Calloway 1
Aerospace Corporation
Post Office Box 92957
Los Angeles, CA 90009

Jerome J. Cuomo 1
T. J. Watson Center
Yorktown Heights, NY 10598

Professor P. H. Fang 1
Department of Physics
Boston College
Chestnut Hill, MA 02167

Wen Hsu 1
Sandia National Laboratories
Division 8347
Box 969
Livermore, CA 94550

Professor W. Lanford 1
Physics Department
S.U.N.Y.
Albany, NY 12222

Professor E. S. Machlin 1
44 Morningstar Drive
Croton-on-Hudson, NY 10520

Michael Pinneo 1
Crystallume
3180 Porter Drive, Suite 2
Palo Alto, CA 94304

Kenneth Russell 1
J. P. L. M. S. 122-123
4800 Oak Grove Drive
Pasadena, CA 91109

Professor T. D. Moustakas 1
Electrical Engineering
Boston University
44 Cummington Street
Boston, MA 02215

Professor J. L. Davidson 1
200 Brown Hall
Auburn University
Auburn, AL 36849

B. Meyerson 1
IBM
T. J. Watson Center
Yorktown Heights, NY 10598

Paul Caldwell 1
DASIAS Field Office
2560 Huntington Avenue
Suite 500
Alexandria, VA 22303

Defense Nuclear Agency 1
ATTN: RAEE (CAPT Fore)
Washington, DC 20305-1000

Dr. Ian Brown 1
Lawrence Berkeley Laboratory
Bldg. 53
University of California
Berkeley, CA 94720

Dr. Andrez Badzian 1
271 Materials Research Laboratory
The Pennslyvania State University
University Park, PA 16802

Prof. Jerzy Bernholc 1
Department of Physics
Box 8202
North Carolina State University
Raleigh, NC 27695-8202

Tarasankar DebRoy 1
Materials Science and Engineering
Penn State University
212 Steidle Building
University Park, PA 16802

Joe Beeler 1
Materials Science and Engineering
Box 7907
North Carolina State University
Raleigh, NC 27695-7907

Michael Frenklach 1
Penn State University
202 Academic Projects Building
University Park, PA 16802

Maurice Landstrass 1
Crystallume
125 Constitution Drive
Menlo Park, CA 94025

Keppi Wu 1
OSD/SDIO/IST
Washington, DC 20301-7100

Warren Pickett 1
Code 4692
Naval Research Laboratory
Washington, DC 20375-5000

Ron Rudder 1
Research Triangle Institute
P. O. Box 12194
Research Triangle Park, NC 27709-2194

John B. Posthill 1
Research Triangle Institute
P. O. Box 12194
Research Triangle Park, NC 27709-2194

Howard Schmidt 1
Schmidt Instruments
2476 Bolsover, Suite 234
Houston, TX 77005

Dr. Skotheim 1
Moltech Corporation
Box 572
Woodville Road
Shoreham, NJ 11786

Karl Spear 1
Pennsylvania State University
201 Steidle
University Park, PA 16802

Max Swanson 1
Department of Physics
University of North Carolina
Chapel Hill, NC 27514

Robert Schwartz 1
NWC Code 38504
Naval Weapons Center
China Lake, CA

T. S. Sudarshan 1
Materials Modification, Inc.
P. O. Box 4817
Falls Church, VA 22044

Wally Yarbrough 1
Penn State University
271 MRL
University Park, PA 16802

Thomas Perry 1
Physics Department
GM Tech Center
Warren, MI 48090

R. Hauge 1
Chemistry Department
Rice University
P. O. Box 1892
Houston, TX 77251

Ken Stalder 1
SRI International
333 Ravenswood Avenue
Menlo Park, CA 94025

C. Richard Guarnieri 1
IBM Research Center
Yorktown Heights, NY 10598

William Banholzer 1
K1-CEB G20, P. O. Box 8
Schenectady, NY 12301

Albert Feldman 1
NIST
Gaithersburg, MD 20899

Dario Narducci 1
IBM Research Division
P. O. Box 219
Yorktown Heights, NY 10598

Prof. Gar B. Hoflund 1
Chemical Engineering
227 Chemical Engineering Building
Gainsville, FL 32611

Dr. A. T. Collins 1
Wheatstone Physics Laboratory
King's College London, Strand
London WC2R 2LS
UNITED KINGDOM

Carl Nelson 1
SDIO/IST
Pentagon
Washington, DC 20301-7100